SECTION C

Geochemistry of igneous suites from the Cajamarca district, northern Peru: Implications for magmatic controls on the formation of porphyry Cu-Au deposits

Section C. Geochemistry of igneous suites from the Cajamarca district, northern Peru: Implications for magmatic controls on the formation of porphyry Cu-Au deposits.

C.1 Abstract

Tertiary igneous rocks in the Cajamarca mining district range from medium to high-K, tholeiitic to calc-alkaline and are predominantly metaluminous. Palaeogene felsic rocks (57-43 Ma) are intermediate in composition (55.6–60.0 SiO_2 wt. %), contain hydrous and anhydrous mineral phases (plagioclase + amphibole + clinopyroxene), and have an average La_N/Yb_N ratio of 8.9. Partial melt modelling suggests these melts equilibrated with a garnet-poor residue that was dominated by pyroxene and olivine. Radiogenic isotope ratios indicate a low ε_{Nd} and high Sr_i material, possibly seawater, contaminated some Palaeogene magmas. Eocene volcanic melt compositions were controlled by fractionation of anhydrous minerals (plagioclase and pyroxene). It is inferred that this igneous suite developed during initial stages of magmatic arc formation and represents immature arc magmas. Oligocene mafic dykes (~29.5 Ma) are dominantly composed of anhydrous phases, have tholeiitic compositions, high ∑REE, and La_N/Yb_N ratios between 4 and 11 (mean = 7). These gabbroic dykes were derived from partial melting of a primitive mantle with an olivine-pyroxene dominated residual mineralogy. The third igneous suite includes Miocene intrusive and volcanic rocks (23.2-8.4 Ma) that were generated during periods of intense crustal thickening. These rocks are characterised by hydrous and anhydrous mineral phases (plagioclase + amphibole ± biotite ± quartz ± clinopyroxene), are intermediate to acidic in composition (57.7–68.8 SiO_2 wt. %) and have steep HREE-depleted profiles. Miocene synmineralisation intrusions are geochemically similar to coeval barren intrusions, but display minor relative enrichment in Th. Partial melting models and radiogenic isotopes indicate Miocene melts were derived from an amphibole-rich upper mantle to lower crust that assimilated minimal upper crustal material. Miocene melts were later strongly influenced by the fractionation of hornblende and biotite. Partial melting models of late Miocene rocks require higher residual garnet (up to 17%) than the early-middle Miocene magmas.

Results from this study suggest variations in residual mineralogy and subsequent fractionation processes are evident in the three igneous suites. These changes in residual mineralogy are inferred to result from an evolving magmatic arc undergoing extensive uplift, rapid increase in crustal thickness and deepening of the mantle-crust boundary. Early-middle Miocene synmineralisation intrusions are related to hydrous melts that were in equilibrium with an amphibole-rich residual, underwent minimal upper crustal contamination and late fractionation of hydrous minerals (i.e. biotite and minor hornblende). In contrast, late Miocene high-sulphidation deposits are linked to HREE-depleted magmas formed during the onset of a flattening subduction angle, cessation of rapid uplift and a progressive change in the residual mineralogy with greater garnet influence.

C.2 Introduction

Porphyry copper deposits form in magmatic arc environments and are related to magmatic fluids that typically exsolve from medium to high K, calc-alkaline magmas emplaced in subvolcanic environments (Sillitoe, 1972, 1988; Burnham, 1979). Numerous studies have characterised the geochemistry, source and evolution of Andean magmatic arc igneous rocks (Hawkesworth *et al*., 1979; Gill, 1981; Hildreth and Moorbath, 1988; Davidson *et al*., 1991; Kay *et al*., 1991; Macfarlane, 1999). In contrast, recent geochemical studies (Lang and Titley, 1998; Richards *et al*., 2001) of porphyry copper deposits have focussed on distinguishing mineralised from non-mineralised intrusive porphyry stocks, as well as defining the residual mineralogy of the source region from which synmineralisation magmas are derived (Kay and Mpodozis, 2001).

The Cajamarca region of northern Peru hosts several Miocene porphyry deposits, including the Michiquillay (Cu-Au-Mo), Minas Conga (Au-Cu), El Galeno (Cu-Au-Mo) Minas Carpa (Au-Cu) and Cerro Corona (Au-Cu) porphyry complexes. A number of high-sulphidation Au deposits are also located in the district, including the Yanacocha Au mine, Sipán, La Zanja and Tantahuatay. Recent studies have characterised mineralised and barren Miocene intrusive stocks in the Hualgayoc district (Macfarlane and Petersen, 1990; Macfarlane *et al*., 1994; James, 1998; Macfarlane, 1999). Whilst Turner (1997) presented major and some trace element data for middle to

late Miocene volcanic rocks in the Yanacocha district. At present, no comprehensive geochemical studies have been reported for the mineralised porphyry centres or regional barren igneous units in the Cajamarca district.

This section presents a petrogenetic model for Tertiary magmatic units in the Cajamarca district. The section includes presentation of new major, trace element and radiogenic isotope data for magmatic units of varying age in the region. This section focuses on identification of different petrogenetic suites, modelling of residual mineralogy and fractionation processes, as well as investigating possible variations between synmineralisation and barren intrusive units. Finally, the petrogenesis of magmatic units in the Cajamarca region is compared with that of other porphyry copper regions located along the Andean belt.

C.3 Tectonic Setting and Regional Geology

The Cajamarca district is situated at an altitude between 2300 and 4400 m in the Western Cordillera of the northern Peruvian Andes where the present day maximum crustal thickness is ~45 km (Fukao *et al*., 1989). It is within one of three major Andean oroclines that is known as the Huancabamba Deflection (Mégard, 1984). The northern part of the deflection zone roughly coincides with the present change in subduction angle of the Nazca plate, from steep slab subduction north of the Peruvian-Ecuador border to shallow (~10^{o}) in central Peru (Fig. 1). The zone of flat subduction in northern and central Peru is defined by the distribution of earthquakes and absence of Quaternary volcanic activity (Barazangi and Isacks, 1979; James, 1981; Jordan *et al*., 1983; James and Sacks, 1999), and has been attributed to a lack of a mantle wedge between the subducting and overriding plate. Gutscher *et al*. (1999) argued that subduction of an ancient oceanic plateau beneath northern Peru occurred from 12 to 10 Ma and resulted in the present day low slab dip angle.

The Cajamarca district is characterised by Cretaceous marine sedimentary rocks that were deformed during Tertiary times by two orogenic episodes, known respectively as the Incaic and Quechua pulses (Mégard, 1984; Benavides, 1999). Initial

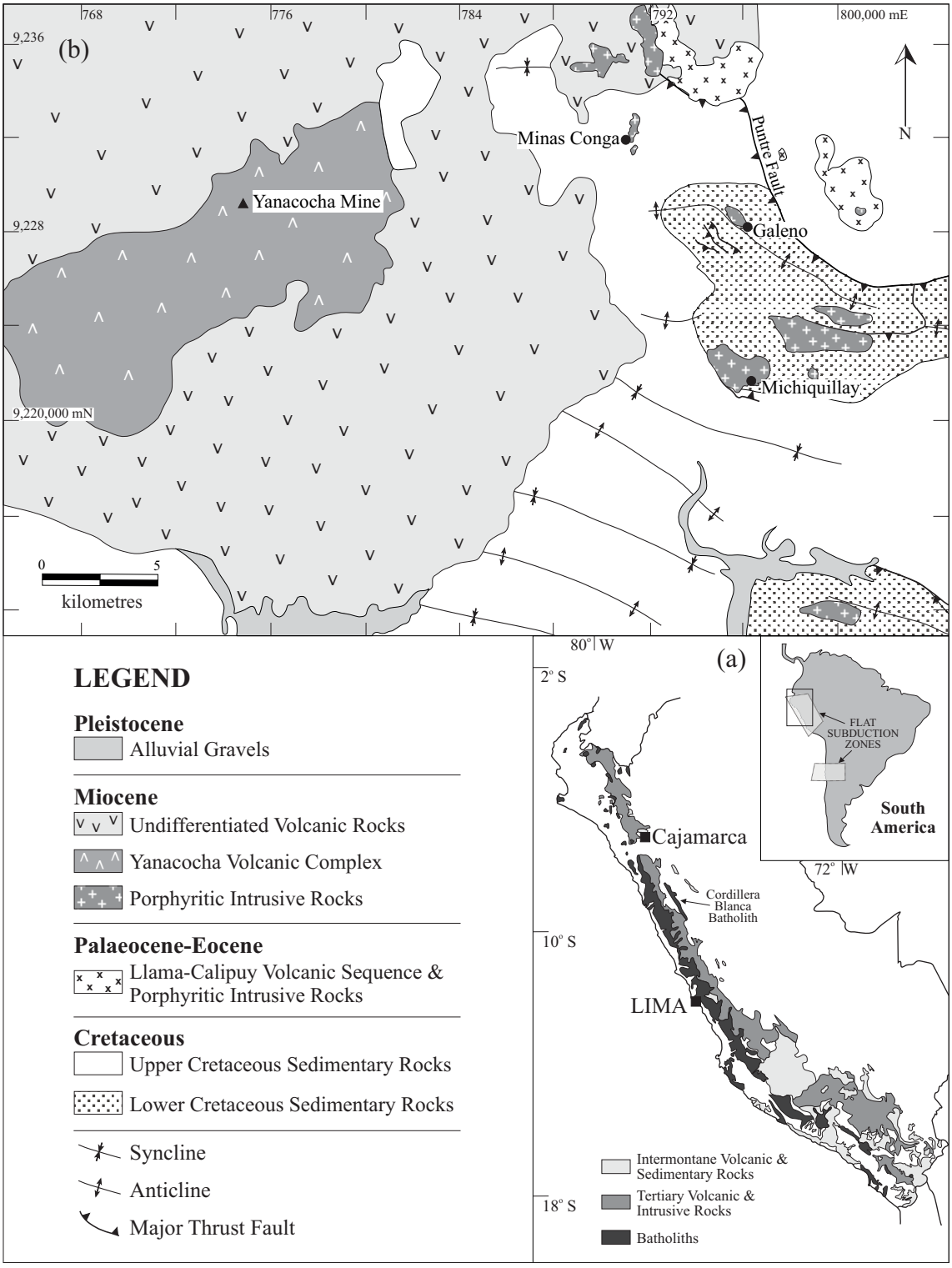

Fig. 1a. Simplified geology of Peruvian Andes showing the major Mesozoic and Cainozoic magmatic rocks. Insert, a map of South America illustrating zones of flat subduction. b. Simplified geological map of the Cajamarca study area (modified from Reyes, 1980).

fold-thrust development during Incaic orogenic pulses (Mégard, 1984) occurred during Eocene times over a reactivated margin of the Brazil shield (Macfarlane, 1999). Igneous rocks in the Cajamarca region are related to three major magmatic episodes that intrude and overlie the deformed Cretaceous sedimentary rocks and metamorphic basement. The first of these magmatic episodes occurred during Palaeogene times (57-35 Ma) and resulted in deposition of the Llama-Calipuy Volcanic Sequence, as well as the emplacement of several intrusive stocks (Noble *et al*., 1990; Section A). The Llama volcanic sequences form an aerially-extensive volcanic succession which is predominantly basaltic to andesitic and ranges in age from 54.8 to 35.4 Ma (Atherton *et al*., 1985; Noble *et al*., 1990; Section A). Oligocene mafic dykes also crop out throughout the region and have been recently dated at 29.4 Ma (Section A).

The second magmatic phase occurred during early-middle Miocene times (~23.2-15.8 Ma). Initiation of this magmatic period coincided with a number of important tectonic events that included a clockwise rotation of the Nazca plate, increased convergence rate, several deformation phases, and major uplift in northern Peru (Pardo-Casas and Molnar, 1987; Noble *et al*., 1990). Based on geophysical and geological data Kono *et al*. (1989) and James and Sacks (1999) concluded that the majority of Miocene crustal thickening in the Western Cordillera resulted from intense magmatism, as opposed to foreshortening in the Eastern Cordillera. This magmatic episode defines the main period of Cu-Au-Mo porphyry formation with the emplacement of several mineralised and barren intrusive units (Llosa *et al*., 1996; Section A). Volcanic rocks related to this magmatic episode are dominantly middle Miocene in age and appear to post-date intrusive activity and porphyry copper formation (Llosa *et al*., 1996; Turner, 1997). This early-middle Miocene magmatic episode in the Cajamarca region was followed by an apparent 3-4 m.y. magmatic hiatus during which extensive intrusive and hydrothermal activity took place to the north of Cajamarca and resulted in formation of the polymetallic deposits in the Hualgayoc mining district (Macfarlane *et al*., 1994; James, 1998).

The final magmatic phase identified near Cajamarca occurred during late Miocene times (12.3 – 8.4 Ma) and was characterised by widespread volcanism incorporating the Yanacocha Volcanic Complex, plus the Regalado and Huambos basalt to andesite volcanic sequences. Evidence for minor intrusive activity, such as

emplacement of tonalite and rhyodacite stocks, has been observed at Yanacocha (Turner, 1997). Formation of the large high-sulphidation Yanacocha Au deposit occurred during this final magmatic interval. Magmatic activity ceased in both the Cajamarca and Hualgayoc districts at approximately 8 Ma (Macfarlane *et al*., 1994; Turner, 1997).

C.4 Analytical Methods

Samples collected and analysed include a diverse compositional range and unaltered or least altered samples were selected where possible. Major, trace and rare earth element analyses of 38 samples from five mineralised intrusive centres, and a variety of barren intrusive plus volcanic units in the Cajamarca region were used in this study (Fig. 2). Major elements and the majority of trace elements (Ba, V, Cr, Co, Ni, Zn, Ga, Rb, Sr, Y, Zr and Nb) were analysed by X-ray fluorescence (XRF) on a Siemens XRF sequential spectrometer (SRS303) and mineral analyses were performed on a Jeol JXA840 electron microprobe at the Advanced Analytical Centre, James Cook University Australia. REE and the remaining trace elements (Cs, Hf, Sc, Ta, Th and U) were analysed by instrumental neutron activation analysis (INAA) at the Becquerel Laboratories, Lucas Heights, New South Wales.

Where possible, unaltered samples were selected for Sr and Nd isotopic analyses. However, this was not always possible and the majority of samples were altered to some degree. Consequently, whole rock powders were leached in hot 6M HCl in a ultrasonicator followed by concentrated HNO_3 on the hotplate for 2 hours to remove any secondary carbonate material that may have perturbed the primary magmatic radiogenic value. The leached material was centrifuged, the HNO_3 removed and the residue was then rinsed with distilled water. Sr and Nd radiogenic isotope results were obtained in static multi-collector mode on a Finnigan-MAT 262 mass spectrometer at La Trobe University, Melbourne, Victoria. Sr isotope ratios were normalised to $^{86}Sr/^{87}Sr = 0.1194$, Nd isotope ratios to $^{146}Nd/^{144}Nd = 0.7219$. Sr isotope data are relative to SRM987-Sr = 0.71024 and Nd isotope data are reported relative to La Jolla-Nd = 0.511860.

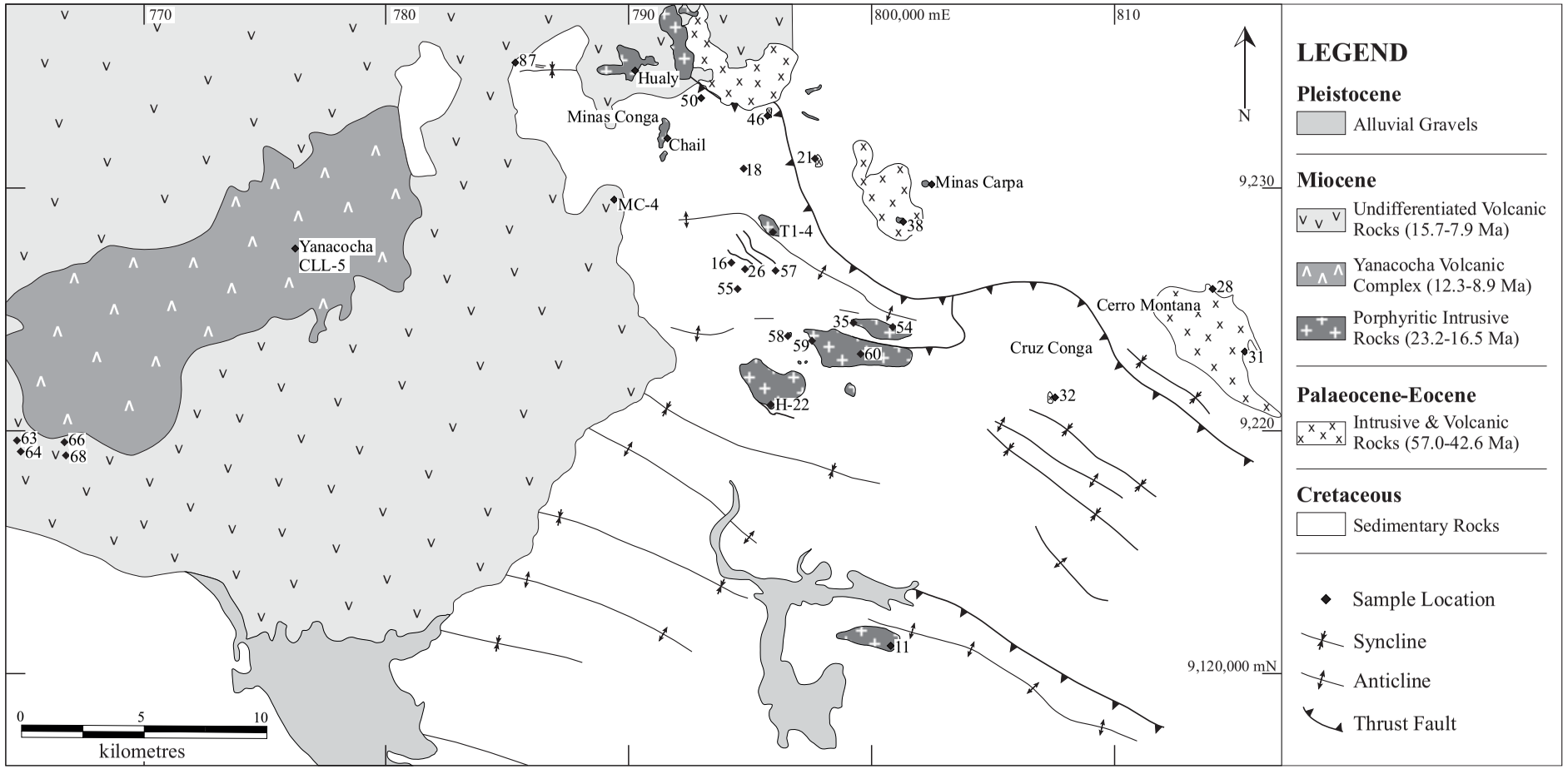

Fig. 2. Simplified geological map of the Cajamarca area showing the locations of the igneous rocks sampled and analysed.

C.5 Petrology - Rock Nomenclature

Tertiary intrusive rocks in the Cajamarca region range from gabbro (rare) to hornblende gabbro (minor) through to hornblende ± biotite diorite (most common). The gabbroic dykes are generally weakly porphyritic, whereas the diorite stocks are moderately to strongly porphyritic in texture. Volcanic sequences in the study area range from basaltic andesite to andesite and are strongly porphyritic. Clinopyroxene is common in the dykes and volcanic units, and generally defines an anhydrous mineral assemblage, i.e. plagioclase + clinopyroxene ± rare hornblende (Fig. 3). The felsic intrusive rocks are mostly characterised by a hydrous mineral assemblage of plagioclase + hornblende ± biotite ± quartz and rare clinopyroxene (Fig. 3). The majority of igneous rocks sampled in the region display weak to moderate alteration, with weak propylitic (sericite-carbonate-chlorite) alteration the most common and widespread.

C.5.1 Gabbroic Dykes

Plagioclase is the most abundant mineral phase in the gabbroic dykes and is present in two size populations with phenocrysts (1-3 mm) generally more abundant (25-75 vol.%, Fig. 3) than microphenocysts (0-50 vol.%; <1 mm). Euhedral plagioclase phenocrysts display both normal (Ca-rich cores) plus reverse (Ca-rich rims) zoning, and are mostly bytownite to labradorite in composition (An_{90-51}, Fig. 4). Euhedral clinopyroxene grains are less abundant (6-8 vol.%), present as phenocrysts (1-3 mm) and microphenocrysts (<1 mm), plus contain reverse zoning textures with Mg-rich rims (Appendix C1). Clinopyroxene grains are dominantly augite (Wo_{40-45}), with the exception of one dyke (S-87) that has augite grains with small, patchy Fe-rich zones (Wo_{39-40}, Fig. 4). Amphibole is present in only two of the samples (S-16 and S-55) and in low abundances (0.5-1.9 vol.%). Amphibole phenocrysts are magnesiohastingsite in composition (Fig. 4) and characterised by high Al_2O_3 and Mg # (67-68), plus low Fe_2O_3(T). These two samples (S-16 and S-55) also contain minor fine-grained phlogopite. The groundmass is feldspathic with fine-grained Fe-Ti oxides (titanomagnetite) and minor apatite present as accessory mineral phases.

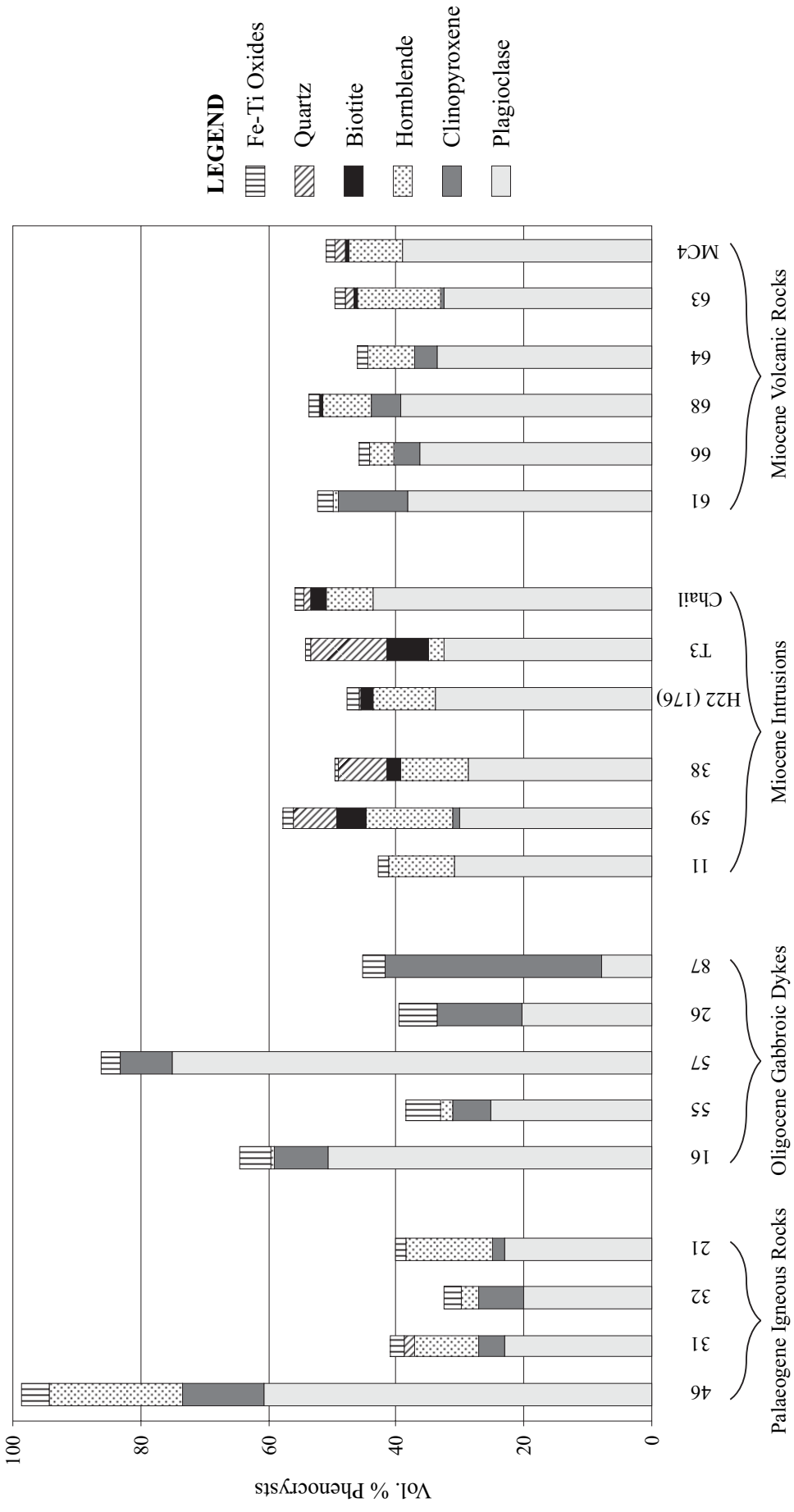

Fig. 3. Phenocryst abundance for the different igneous suites.

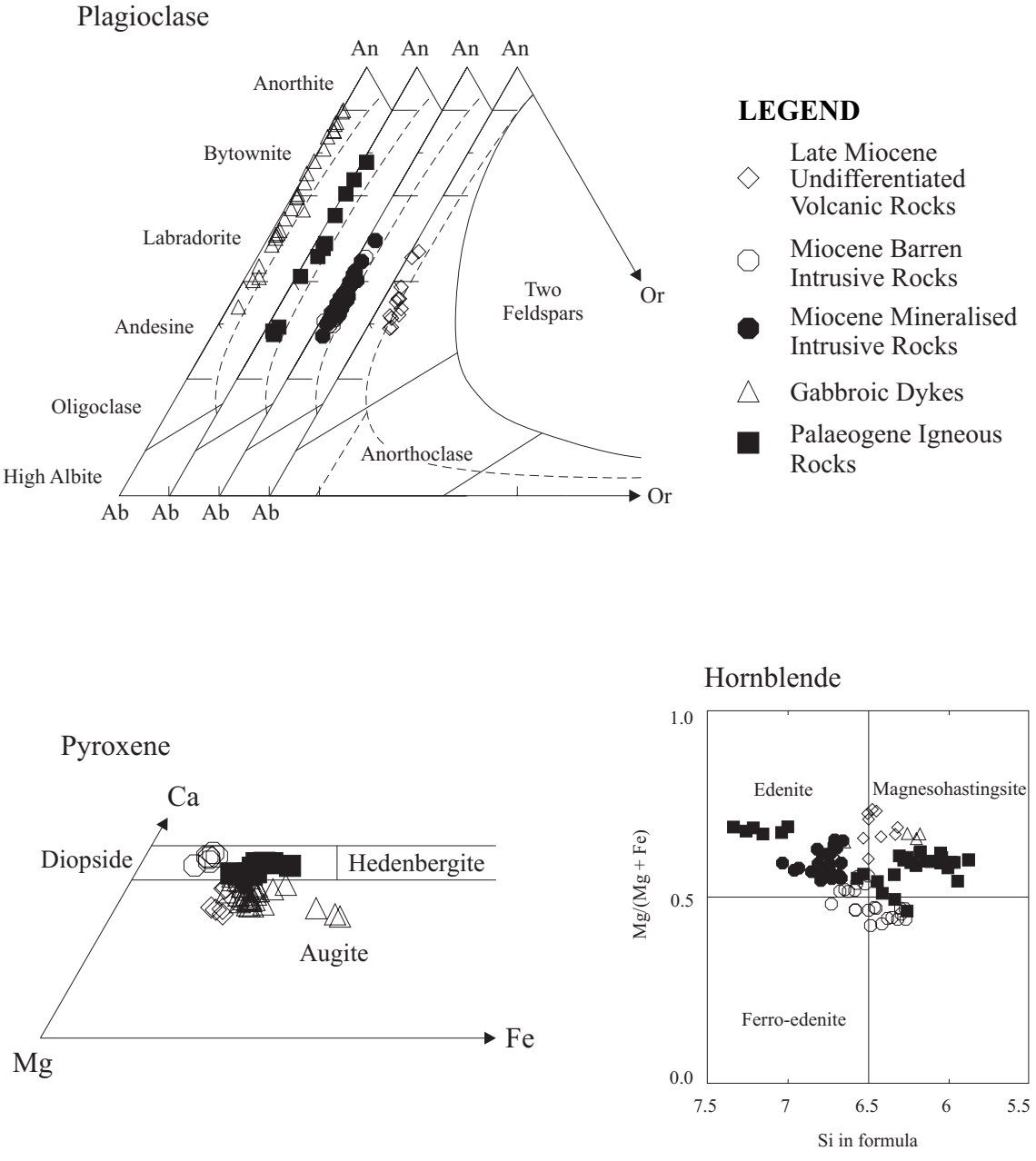

Fig. 4. Mineral chemistry and classification diagrams for pyroxene, hornblende and plagioclase phenocrysts.

C.5.2 Felsic Intrusive Units

Palaeogene and Miocene felsic intrusive bodies display similar petrographic characteristics with euhedral plagioclase the most abundant phenocryst (1-7 mm; 23-61 vol.%, Fig. 3). Plagioclase is characterised by normal, reverse and oscillatory zoning (Fig. 5), and some grains from mineralised centres have albite-sericite altered rims. Plagioclase phenocrysts from Palaeogene intrusive units range from bytownite to andesine (An_{74-34}; 23-61 vol.%), whereas phenocrysts from Miocene intrusive centres are dominantly less calcic and plot between labradorite and andesine (An_{57-38}; 25-44 vol.%, Fig. 4). Calcic amphibole phenocrysts (1-8 mm) in the felsic intrusive rocks are predominantly euhedral, light yellow to light brown or green in thin section and may contain minor feldspar inclusions. Amphiboles from barren Palaeogene intrusions are dominantly magnesiohastingsite to pargasite (Mg # = 51-69; 10-21 vol.%). Amphibole phenocrysts from barren Miocene intrusive centres tend to have lower SiO_2, MgO and higher Fe_2O_3(T) (Mg # = 42-56; 11-13 vol.%) than amphiboles from mineralised centres that are commonly edenites (Mg # = 47-65; 1-9 vol.%). Euhedral magmatic biotite phenocrysts (Mg # = 57-66; 2-6 vol.%) are present in all mineralised centres and range in size from 0.5 to 3 mm. Biotite phenocrysts have a low abundance in barren intrusive units (0-5 vol.%) and are strongly chloritised. Rounded quartz phenocrysts (1-4 mm) are present in some rocks and contain minor embayments. Euhedral clinopyroxene grains (0.5-2.0 mm) in samples S-59, S-31 and S-28 are present in minor amounts (1-4 vol.%). Clinopyroxenes from one hornblende-biotite quartz diorite (S-59) are diopsides (Wo_{47-49}) and have higher Mg # (Mg # = 81-86) than those from the gabbroic dykes (Appendix C1). Phenocrysts are set in a feldspathic groundmass. Zircon, apatite and Fe-Ti oxide (titanomagnetite) are present as accessory phases.

C.5.3 Volcanic Sequences

Rocks from the Lower Llama Volcanic Formation (~43 Ma; S-21 and S-32) contain euhedral plagioclase, hornblende and clinopyroxene phenocrysts set in a feldspathic groundmass with a trachytic texture. Euhedral plagioclase phenocrysts (0.3-1.0 mm; 20-23 vol.%) are the dominant phenocryst phase in S-32 and range in composition from An_{78} to An_{57}. Euhedral clinopyroxene phenocrysts (Mg # = 62-71; 2–7 vol.%) are less abundant, characterised by very high TiO_2 and Al_2O_3 contents (Appendix C1), and are diopsides (Wo_{45-47}). Some clinopyroxene grains display zoned and/or twinned textures. Amphibole phenocrysts from S-32 (Mg # = 59-62; 3 vol.%) are

Fig. 5. Backscattered image of a plagioclase phenocryst from a mineralised centre (Sample S-T2: GN-39 214m). The image illustrates the oscillatory zonation of some plagioclase phenocrysts with Ca-rich zones appearing grey and the Ca-Na-rich zones having a light grey appearance. The phenocryst is set in a feldspathic groundmass with spotted quartz (dark grey) and K-feldspar (light grey). Width of image is 950 μm.

pargasites with high TiO_2 and Al_2O_3 plus low SiO_2 (Appendix C1). Amphiboles in S-21 are magnesiohastingsite to hastingsite and characterised by high Fe_2O_3(T) and Al_2O_3, plus low SiO_2 and Mg # (Mg # <62; 13 vol.%). Apatite microphenocrysts (0.1-0.3 mm; 1 vol.%) are also present in both samples.

Basaltic andesite rocks of the Regalado Volcanic Formation (~12.3 Ma; S-61, S-64, S-66, S-68) contain plagioclase (0.3-5.0 mm), clinopyroxene (0.2-1.5 mm) and amphibole (0.2-6.0 mm) phenocrysts. Euhedral plagioclase (34-39 vol.%; An_{58-41}) phenocrysts are characterised by normal, reverse and strong oscillatory zonation patterns. Amphibole phenocrysts (1-7 vol.%) have generally low Fe_2O_3(T) and high MgO, which reflect relatively high Mg # (58 to 74) compared with the felsic intrusive units. Amphibole phenocrysts are commonly poikilitic with feldspar, clinopyroxene and Fe-Ti oxide inclusions. Rims of amphibole grains have been altered to hematite. Euhedral clinopyroxene phenocrysts are generally less abundant (4–10 vol.%), commonly twinned and have high Mg # (> 75). They are typically diopside (Wo_{43-39}) and slightly depleted in Al_2O_3 plus Fe_2O_{3T}. The groundmass is felspathic and glassy with euhedral apatite microphenocrysts (0.1 mm) present in minor amounts (0.2-0.3 vol.%).

Andesite rocks from the Huambos volcanic sequences (~8 Ma; S-63 and S-MC4) consist of plagioclase, biotite, hornblende, quartz and clinopyroxene phenocrysts set in a feldspathic groundmass. Plagioclase phenocrysts (33-39 vol.%) display complex zoning patterns and are andesine in composition (An_{50-43}). Euhedral amphibole phenocrysts (8.5-13.0 vol.%) tend to have rims partially altered to hematite, low Fe_2O_3(T) and high MgO with Mg # of 56-73. Quartz phenocrysts (1.6 vol.%) are rounded and generally have minor embayments. Euhedral biotite phenocrysts (Mg# = 57-64; 0.6-0.7 vol.%) are enriched in Na_2O but depleted in K_2O compared with biotite phenocrysts from mineralised intrusive centres (Appendix C1). Clinopyroxene phenocrysts are rare, subhedral to euhedral, have low TiO_2 and are augites (Mg # = 72).

In summary, the rocks from the Eocene Llama Volcanic Sequence (S-21 and S-32) are characterised by amphiboles and clinopyroxenes that are enriched in TiO_2 and Al_2O_3 but depleted in SiO_2 compared to minerals from the Miocene Regalado and Huambos Formations.

C.6 Major Elements

The igneous rocks show a broad range in SiO_2 concentration (47.9–68.8 wt% SiO_2) and a large range in loss on ignition (11.3–0.9 wt% LOI; Appendix C2). Major component analyses have been normalised 100% on a volatile-free basis to facilitate comparison (Table 1). The gabbroic dykes are dominantly more basic [47.9–52.4 wt% $SiO_{2(N)}$] than the Palaeogene igneous units that are intermediate in composition [55.6–60.0 wt% $SiO_{2(N)}$] and the Miocene units range from intermediate to acidic [57.7-68.8 wt% $SiO_{2(N)}$]. The majority of intrusive and volcanic samples plot in the medium to high-K field (Fig. 6), range from weakly alkaline to subalkaline, and are metaluminous. The gabbroic dykes straddle the tholeiite - calc-alkaline boundary displaying a high Fe_2O_3(T) content, whereas the other igneous rocks show calc-alkaline affinity (Fig. 6).

The gabbroic dykes display increasing TiO_2, Na_2O and K_2O with fractionation, as monitored by SiO_2 (Fig. 7) and MgO. Fe_2O_3(T), CaO and MgO decrease with increasing SiO_2 for the gabbroic units, with Al_2O_3 and P_2O_5 displaying minor scatter. In general, the gabbros display a large amount of scatter that is possibly related to the moderate alteration and element mobility. Palaeogene felsic rocks show negative correlations of silica with TiO_2, Fe_2O_3(T), CaO and MgO. One volcanic sample (S-32) has anomalously high TiO_2. The remaining major elements, Al_2O_3, Na_2O, K_2O, MnO and P_2O_5, increase with increasing fractionation. Miocene intrusive and volcanic units show linear negative correlations between TiO_2, MgO and P_2O_5 and silica, whereas CaO, Fe_2O_3(T) and possibly Na_2O show curvilinear negative correlations. SiO_2 and K_2O display a positive curvilinear correlation, whereas Al_2O_3 shows no clear correlation with silica. Mineralised Miocene centres display similar major element trends and contents to barren intrusive centres of similar age with the exception of K_2O, which shows slight enrichment in the mineralised systems. This enrichment is probably due to hydrothermal alteration as evident from a K-feldspar-biotite altered sample from the El Galeno prospect (S-T1) that has an abnormally high K_2O/Al_2O_3 ratio. Fractionation trends are difficult to accurately determine due to the amount of scatter associated with phenocryst-rich units and partial alteration overprint. However, trends for CaO, K_2O

Table 1. Whole rock geochemistry of Tertiary igneous rocks in the Cajamarca region. Major components have been normalised on a volatile-free basis.

Suite	**Gabbroic Dykes**						**Palaeocene-Eocene Intrusions**				**Eocene - Llama Volcanic**			
Locality	S Galeno	S Galeno	S Galeno	N Galeno	E Galeno	N Galeno	Cerro Montana		East Minas Conga		La Carpa	Cruz Conga	Aurora Patricia	La Carpa
Sample No.	S-16	S-55	S-57	S-18	S-26	S-87	S-28	S-31	S-46	S-50	S-21	S-32	S-11	S-38
Rock Type	Hbl Gabbro	Hbl Gabbro	Gabbro	Gabbro	Gab Diorite	Gab Diorite	Hbl Diorite	Hbl Diorite	Hbl MD	Hbl MD	Hbl Andesite	Hbl Bas Andesite	Hbl Diorite	Hbl Qtz Diorite
wt. %														
SiO_2	48.88	47.89	50.35	48.65	52.11	52.41	59.99	58.23	55.88	55.60	57.57	56.37	62.87	65.33
TiO_2	1.26	1.15	1.30	1.34	1.55	1.12	0.59	0.66	0.71	0.71	0.65	1.13	0.53	0.49
Al_2O_3	19.08	18.23	20.17	18.47	17.34	18.59	18.01	19.04	17.84	18.24	19.00	18.92	17.88	17.08
$Fe_2O_3(T)$	12.18	13.18	10.07	11.48	11.40	10.37	7.19	7.66	7.40	8.02	6.61	7.06	4.95	3.99
MnO	0.17	0.23	0.21	0.14	0.66	0.15	0.30	0.27	0.17	0.17	0.22	0.25	0.11	0.08
MgO	5.11	5.08	3.88	7.02	3.91	3.40	1.90	2.05	3.69	4.06	2.11	1.66	1.85	1.84
CaO	9.89	10.83	9.60	9.06	7.11	9.41	5.54	5.15	8.20	7.84	6.92	6.59	5.85	4.63
Na_2O	2.26	2.40	3.29	3.25	3.22	3.31	3.94	4.86	3.82	3.98	4.51	4.67	3.77	3.84
K_2O	0.99	0.79	0.95	0.21	2.17	0.96	2.13	1.72	2.06	1.14	2.09	2.86	1.95	2.51
P_2O_5	0.18	0.22	0.18	0.38	0.53	0.26	0.40	0.37	0.23	0.25	0.31	0.47	0.24	0.21
$Total_{(N)}$	100.00	100.00	100.00	100.00	100.00	100.00	100.00	100.00	100.00	100.00	100.00	100.00	100.00	100.00
LOI	5.66	7.71	2.60	11.31	3.10	3.18	3.94	2.89	0.92	4.65	2.06	3.15	3.08	2.92
ppm														
Cr	19	9	5	39	36	3	9	19	31	10	0	0	26	21
Ni	13	13	14	32	28	8	9	6	15	16	6	5	6	11
Co	40	33	29	30	32	24	12	11	27	22	19	17	13	17
Sc	25	18	21	25	22	18	6	7	18	18	8	5	7	7
V	332	291	222	247	185	184	42	62	174	187	114	82	70	79
Rb	35	14	24	<1	67	18	61	39	62	27	59	74	60	76
Cs	8	1	2	<1	8	<1	<1	1	6	1	2	<1	1	3
Ba	375	366	621	829	701	373	1228	580	803	648	902	1073	827	864
Sr	514	582	711	625	472	571	898	799	635	816	775	967	584	623
Ga	17	17	23	18	21	16	16	16	20	19	20	23	21	21
Ta	<1	<1	1.04	<1	1.77	<1	<1	1.05	<1	<1	<1	2.17	<1	<1
Nb	1	2	9	11	21	4	3	7	5	4	5	29	5	5
Hf	1.9	1.8	2.1	2.4	5.1	3.5	3.6	3.3	2.9	2.6	3.6	5.0	3.1	3.0
Zr	51	57	81	88	241	128	112	97	86	83	111	189	110	92
Y	19	19	17	18	37	27	73	27	21	19	25	28	17	16
Th	1.5	1.7	3.4	3.5	9.6	3.0	3.2	4.7	6.9	5.5	7.3	12.0	4.6	3.0
U	<2	<2	<2	<2	3.1	<2	<2	<2	<2	<2	2.1	2.4	<2	2.2
La	10.60	12.70	18.40	24.30	43.20	20.00	34.00	25.80	25.90	23.60	34.10	58.40	20.70	15.00
Ce	22.70	25.30	36.10	47.10	82.40	46.00	60.70	51.00	48.00	44.30	65.10	106.00	37.30	26.70
Nd	13.10	13.00	16.90	na	35.10	na	32.20	25.30	23.00	na	26.60	41.50	18.00	14.70
Sm	3.15	3.26	3.39	4.32	7.14	5.07	7.54	5.42	4.09	3.96	5.50	7.26	3.66	3.40
Eu	1.11	1.02	1.33	1.26	1.71	1.42	2.50	1.74	1.17	0.84	1.58	2.07	1.03	0.75
Tb	0.62	0.54	0.65	0.60	1.10	0.88	1.32	0.90	0.69	0.64	0.78	0.94	0.51	0.48
Ho	0.74	0.69	0.77	na	1.28	na	1.78	1.07	0.85	na	0.98	1.13	0.58	na
Yb	1.77	1.67	1.60	1.48	3.16	2.64	4.45	2.59	2.05	1.88	2.70	2.42	1.27	0.86
Lu	0.24	0.23	0.22	0.21	0.45	0.40	0.66	0.35	0.29	0.28	0.34	0.31	<0.20	<0.20
Rb/Sr	0.07	0.02	0.03	0.00	0.14	0.03	0.07	0.05	0.10	0.03	0.08	0.08	0.10	0.12
Sr/Y	27.1	30.6	41.8	34.7	12.8	21.1	12.3	29.6	30.2	42.9	31.0	34.5	34.4	38.9
Zr/Nb	51.0	28.5	9.0	8.0	11.5	32.0	37.3	13.9	17.2	20.8	22.2	6.5	22.0	18.4
La_N/Yb_N	4.0	5.1	7.7	11.0	9.1	5.1	5.1	6.7	8.4	8.4	8.4	16.1	10.9	11.7

$Total_{(N)}$ = Volatile-free normalised; <2 = below detection limit; na = not analysed
Gab Diorite = Gabbroic Diorite; MD = Microdiorite; Bas Andesite = Basaltic Andesite; Hbl = Hornblende; Bt = Biotite

Table 1. cont.

Suite	Miocene Barren Intrusions							Miocene Synmineralisation Intrusions							
Locality	Michiquillay Region						Galeno Prospect	Michiquillay Prospect			Minas Conga Prospect		Galeno Prospect		
Sample No.	S-35	S-36	S-54	S-58	S-59	S-60	S-T4	S-H22(244)	S-H22(176)	S-H22(180)	S-Chail	S-Hualy	S-T1	S-T2	S-T3
Rock Type	Hbl-Bt Diorite	Hbl-Bt Diorite	Hbl-Bt Diorite	Hbl-Bt Diorite	Hbl-Bt Qtz Diorite	Hbl-Bt Diorite	Hbl-Bt Diorite	Hbl-Bt Diorite	Hbl-Bt Diorite	Hbl-Bt Diorite	Hbl-Bt Diorite	Hbl-Bt Diorite	Hbl-Bt Diorite	Hbl-Bt Diorite	Hbl-Bt Qtz Diorite
wt. %															
SiO_2	61.05	63.45	63.83	60.69	60.74	62.95	59.56	64.39	62.74	63.92	63.34	63.26	66.40	68.08	65.24
TiO_2	0.62	0.58	0.56	0.64	0.66	0.57	0.61	0.56	0.57	0.57	0.51	0.58	0.50	0.49	0.47
Al_2O_3	17.57	16.99	16.99	17.38	17.42	17.78	16.55	18.18	17.18	16.70	17.42	17.30	18.13	17.74	16.81
$Fe_2O_3(T)$	5.54	4.88	4.83	5.77	5.71	5.06	7.97	4.87	5.24	5.72	4.78	5.15	3.64	2.36	4.49
MnO	0.12	0.11	0.10	0.12	0.12	0.12	0.07	0.25	0.08	0.00	0.09	0.18	0.00	0.00	0.10
MgO	2.50	1.98	1.96	2.74	2.72	1.59	4.50	0.98	2.29	2.30	1.74	2.47	1.70	1.40	1.60
CaO	6.62	6.25	5.93	6.31	6.28	5.88	4.76	5.12	5.55	4.41	5.07	5.99	0.61	2.38	4.29
Na_2O	3.77	3.33	3.28	4.09	4.10	3.90	3.62	2.64	3.74	3.72	4.33	3.61	2.74	3.55	3.39
K_2O	1.98	2.20	2.29	2.04	2.02	1.92	2.15	2.78	2.37	2.41	2.48	1.23	6.10	3.77	3.39
P_2O_5	0.23	0.24	0.23	0.23	0.23	0.23	0.20	0.24	0.23	0.23	0.23	0.22	0.18	0.24	0.21
$Total_{(N)}$	100.00	100.00	100.00	100.00	100.00	100.00	100.00	100.00	100.00	100.00	100.00	100.00	100.00	100.00	100.00
LOI	2.22	5.08	5.63	4.47	2.50	3.62	2.12	7.80	1.40	1.84	1.32	5.06	4.31	3.83	2.60
ppm															
Cr	29	12	7	43	28	7	175	5	45	42	33	41	35	35	46
Ni	12	8	7	20	12	6	46	4	13	12	9	11	10	5	8
Co	24	15	19	17	22	15	23	24	23	22	21	14	21	20	21
Sc	10	8	8	13	13	7	18	10	10	10	8	8	6	6	6
V	103	95	93	123	118	87	146	79	90	94	72	116	80	79	68
Rb	58	64	66	60	60	52	90	100	51	75	72	33	165	81	88
Cs	<1	2	4	3	2	-1	3	3	1	2	<1	1	4	5	2
Ba	708	893	1065	622	671	766	344	529	668	582	723	473	630	606	794
Sr	793	625	580	619	708	774	532	230	690	600	643	615	295	491	528
Ga	20	18	19	19	19	20	20	21	18	20	19	20	18	18	20
Ta	<1	<1	<1	<1	<1	<1	<1	<1	1.46	1.18	1.21	<1	<1	1.26	<1
Nb	5	6	5	4	4	6	4	6	7	7	5	6	6	7	7
Hf	2.5	2.9	3.4	2.3	2.7	2.8	2.5	3.0	3.0	3.1	3.4	3.0	2.7	3.2	2.4
Zr	78	82	89	84	81	87	67	95	70	82	93	63	99	85	62
Y	12	11	16	12	15	11	16	16	14	12	13	13	13	11	10
Th	4.2	4.3	4.1	3.7	4.5	4.1	3.8	6.2	5.8	6.1	6.1	5.8	3.8	4.6	5.1
U	<2	2.7	<2	<2	<2	<2	<2	<2	<2	<2	<2	<2	<2	<2	<2
La	15.90	16.70	19.90	15.10	17.20	17.50	14.70	17.50	16.90	16.90	19.30	17.20	14.40	19.60	16.40
Ce	36.10	32.90	37.60	31.40	36.40	37.10	29.70	37.40	35.60	33.90	37.70	33.90	30.40	39.90	32.50
Nd	na	na	na	na	16.90	na	15.60	na	16.90	15.80	17.40	16.30	16.20	20.10	15.50
Sm	3.82	3.54	4.16	3.41	3.49	4.01	3.46	3.56	3.40	2.91	3.28	3.18	3.40	3.77	2.97
Eu	1.23	1.06	1.23	1.03	0.98	1.16	1.17	0.94	1.03	0.89	0.95	0.80	0.98	0.96	0.89
Tb	0.53	0.52	0.60	0.50	0.53	0.53	0.55	0.52	0.45	0.38	0.47	0.48	0.48	0.48	0.43
Ho	na	na	na	na	0.62	na	0.65	na	0.49	0.45	0.57	0.54	0.48	0.46	0.44
Yb	0.86	0.91	1.14	1.12	1.21	0.88	1.32	1.21	0.96	0.93	1.20	1.11	0.91	0.79	0.78
Lu	<0.20	<0.20	<0.20	<0.20	<0.20	<0.20	<0.20	<0.20	<0.20	<0.20	<0.20	<0.20	<0.20	<0.20	<0.20
Rb/Sr	0.07	0.10	0.11	0.10	0.08	0.07	0.17	0.43	0.07	0.13	0.11	0.05	0.56	0.16	0.17
Sr/Y	66.1	56.8	36.3	51.6	47.2	70.4	33.3	14.4	49.3	50.0	49.5	47.3	22.7	44.6	52.8
Zr/Nb	15.6	13.7	17.8	21.0	20.3	14.5	16.8	15.8	10.0	11.7	18.6	10.5	16.5	12.1	8.9
La_N/Yb_N	12.4	12.3	11.7	9.0	9.5	13.3	7.4	9.7	11.8	12.2	10.8	10.4	10.6	16.6	14.1

Table 1. cont.

Suite			Regalado Volcanic Units (M-L Mio)				Huambos Volcanics (L Mio)	
Locality	Minas Carpa	Yanacocha	North Cajamarca				W M Conga	
Sample No.	S-M Carpa	S-CLL5	S-61	S-64	S-66	S-68	S-63	S-MC4
Rock Type	Hbl-Bt Diorite	Hbl-Bt Diorite	Hbl Bas Andesite	Hbl Bas Andesite	Hbl Bas Andesite	Hbl Bas Andesite	Hbl-Bt Andesite	Hbl-Bt Andesite
wt. %								
SiO_2	65.03	68.78	57.74	62.49	59.66	57.86	60.05	62.93
TiO_2	0.51	0.38	0.71	0.58	0.69	0.76	0.71	0.55
Al_2O_3	17.04	17.07	18.47	17.46	18.09	18.37	17.98	17.12
Fe_2O_3(T)	5.88	2.08	6.43	5.46	5.98	6.82	5.78	5.08
MnO	0.07	0.00	0.14	0.11	0.10	0.21	0.10	0.16
MgO	1.81	1.13	3.35	1.97	2.84	2.68	2.47	2.27
CaO	2.99	2.71	7.27	5.84	6.67	7.59	6.51	5.20
Na_2O	3.55	4.74	4.11	3.67	3.92	3.80	4.25	4.09
K_2O	2.89	2.92	1.52	2.17	1.77	1.63	1.88	2.38
P_2O_5	0.23	0.18	0.25	0.24	0.27	0.29	0.27	0.22
$Total_{(N)}$	100.00	100.00	100.00	100.00	100.00	100.00	100.00	100.00
LOI	4.06	1.18	1.18	3.95	1.58	2.55	1.21	2.72
ppm								
Cr	35	44	22	13	10	11	25	0
Ni	6	5	16	10	12	11	14	9
Co	22	26	23	20	19	18	19	21
Sc	8	5	17	13	13	13	10	9
V	87	68	132	102	120	129	123	101
Rb	87	83	33	64	46	42	47	70
Cs	3	<1	<1	<1	1	<1	2	<1
Ba	617	895	620	610	534	488	560	1973
Sr	433	805	838	660	718	759	820	594
Ga	20	20	21	19	22	21	22	20
Ta	<1	1.04	<1	<1	<1	<1	<1	<1
Nb	7	2	1	4	3	3	3	5
Hf	3.2	3.6	2.7	2.9	3.2	3.2	2.8	2.5
Zr	93	94	83	86	101	95	105	84
Y	14	7	18	20	15	14	16	12
Th	6.3	6.1	2.5	3.7	3.8	3.2	5.9	6.3
U	<2	<2	<2	<2	<2	<2	2.2	2.2
La	18.30	20.20	18.20	20.50	18.60	17.90	22.30	18.20
Ce	36.80	39.00	36.10	42.00	37.80	38.40	41.60	35.50
Nd	17.10	16.50	17.60	na	na	na	19.70	na
Sm	3.28	2.62	3.81	4.00	4.00	3.98	3.90	3.41
Eu	1.06	0.78	1.11	1.05	1.01	0.81	1.15	0.57
Tb	0.45	0.33	0.62	0.61	0.62	0.50	0.60	<0.50
Ho	0.52	0.35	0.77	na	na	na	0.74	na
Yb	1.12	0.62	1.65	1.23	1.37	1.29	1.56	0.99
Lu	<0.20	<0.20	0.21	<0.20	0.20	<0.20	0.22	<0.20
Rb/Sr	0.20	0.10	0.04	0.10	0.06	0.06	0.06	0.12
Sr/Y	30.9	115.0	46.6	33.0	47.9	54.2	51.3	49.5
Zr/Nb	13.3	47.0	83.0	21.5	33.7	31.7	35.0	16.8
La_N/Yb_N	10.9	21.8	7.4	11.1	9.1	9.3	9.6	12.3

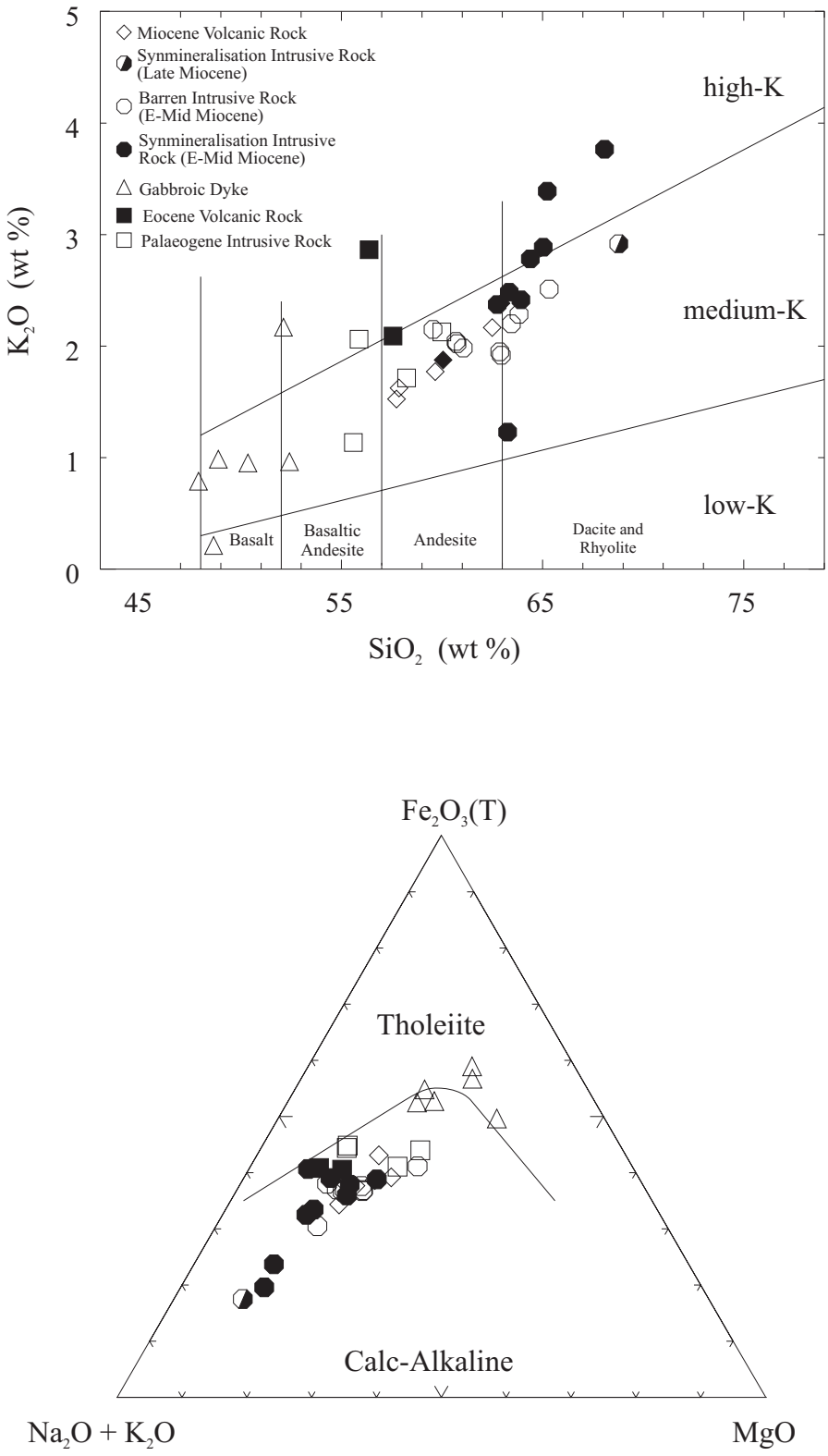

Fig. 6. K_2O vs. SiO_2 variation diagram for subalkaline rocks (Le Maitre *et al*., 1989). Tholeiite vs. calc-alkaline plot from Irvine and Baragar (1971).

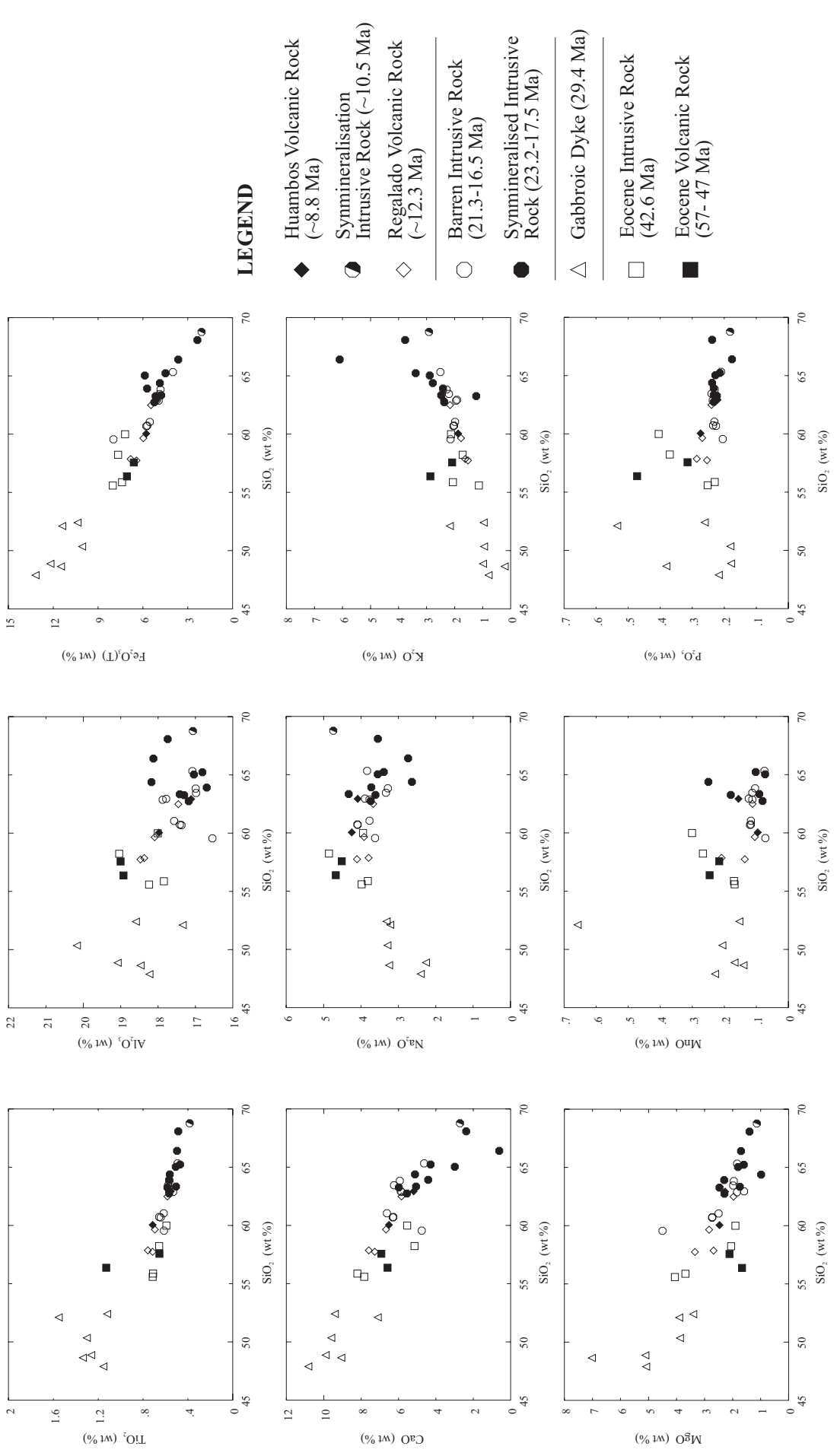

Fig. 7. Major element vs. SiO_2 variation diagrams for igneous rocks in the Cajamarca region.

and MgO against SiO_2 in all the igneous units are suggestive of fractionation of clinopyroxene, plagioclase, amphibole and titanomagnetite.

C.7 Trace Elements

The igneous units as a whole display an overall decrease in compatible elements Ni, Sc and V with increasing fractionation (as monitored by SiO_2; Fig. 8). One sample (S-T4) has anomalously high Cr and Ni contents (Table 1). Palaeogene felsic units display significantly steeper trends of decreasing Ni and Co than the other igneous suites. Large ion lithophile elements (LILE) Rb and Ba increase with fractionation in all igneous suites. High Rb content in sample S-T1 is due probably to alteration of plagioclase phenocrysts and an anomalously high Ba content is also evident in a late Miocene volcanic sample (S-MC4). Samples from mineralised centres are slightly depleted in Ba compared to coeval barren intrusive units, which possibly reflects Ba mobility during hydrothermal activity. Palaeogene felsic rocks display a slight increase in Sr content with fractionation compared to the Miocene units that show a steep decrease. A plot of Rb/Sr vs SiO_2 (Fig. 8) for all the igneous units displays moderate scatter but an overall increase in the Rb/Sr ratio associated with increasing silica content. Palaeogene felsic and Oligocene basic rocks display an overall increase in high field strength elements (HFSE) Nb, Hf and Zr with fractionation. Two samples (S-26 and S-32) display anomalously high HFSE values. Th and SiO_2 correlate negatively in the Palaeogene units. With the exception of the three samples from El Galeno, synmineralisation intrusions are typically enriched in Th compared with coeval barren intrusive units. Samples from El Galeno contain slightly lower Th than other samples from mineralised centres. La and SiO_2 show positive correlations in both the dykes and Palaeogene felsic rocks. However, the more evolved Miocene units display limited variation with increasing SiO_2. Heavy rare earth elements (HREE) and Y also display a positive correlation with increasing fractionation for the dykes and Palaeogene felsic units, but the Miocene units display a negative correlation. MORB normalised trace element diagrams dominantly show depletion in HFSE relative to LILE, as well as marked troughs for Nb, Ti and Rb (Fig. 9).

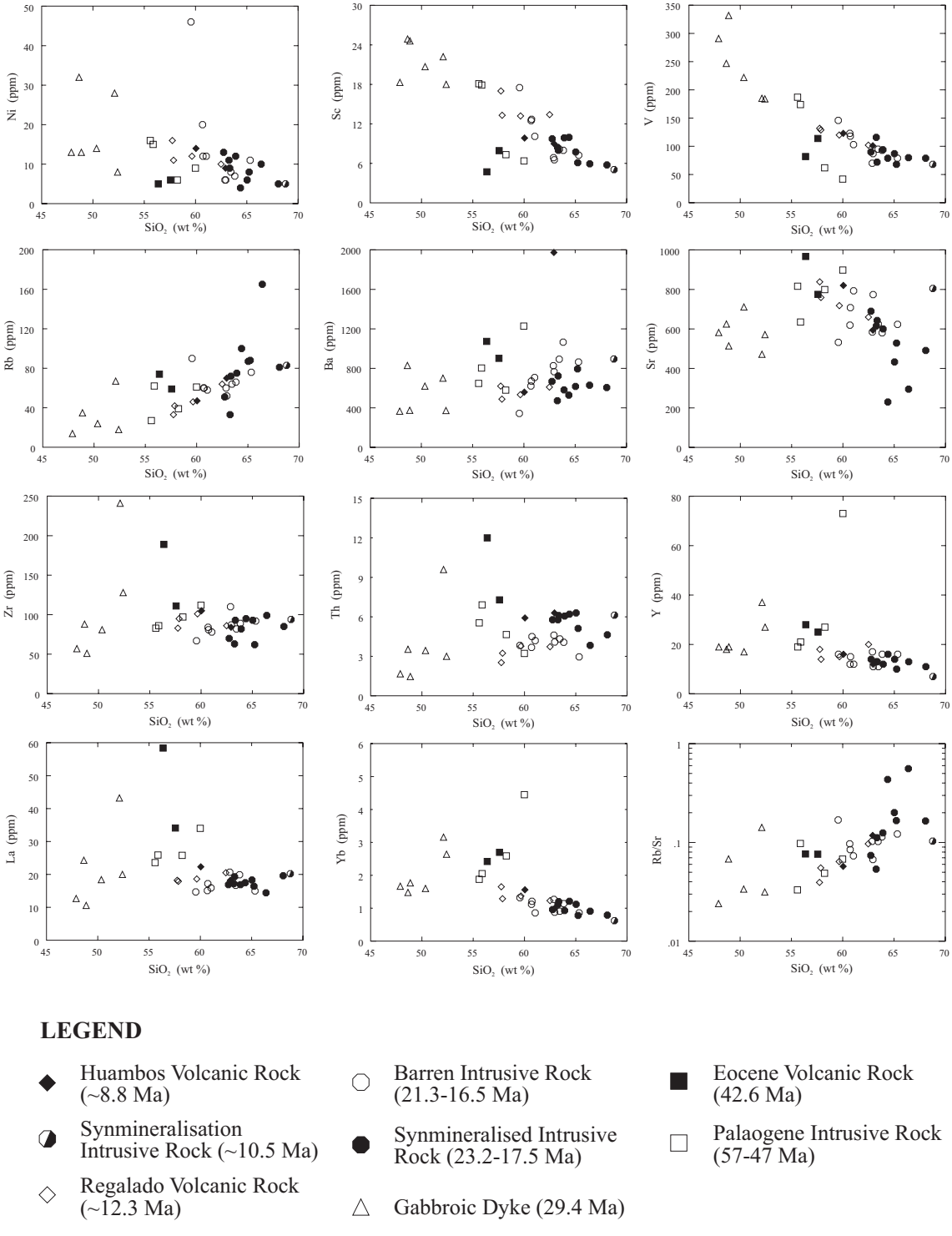

Fig. 8. Trace element vs. SiO_2 variation diagrams for igneous rocks in the Cajamarca region.

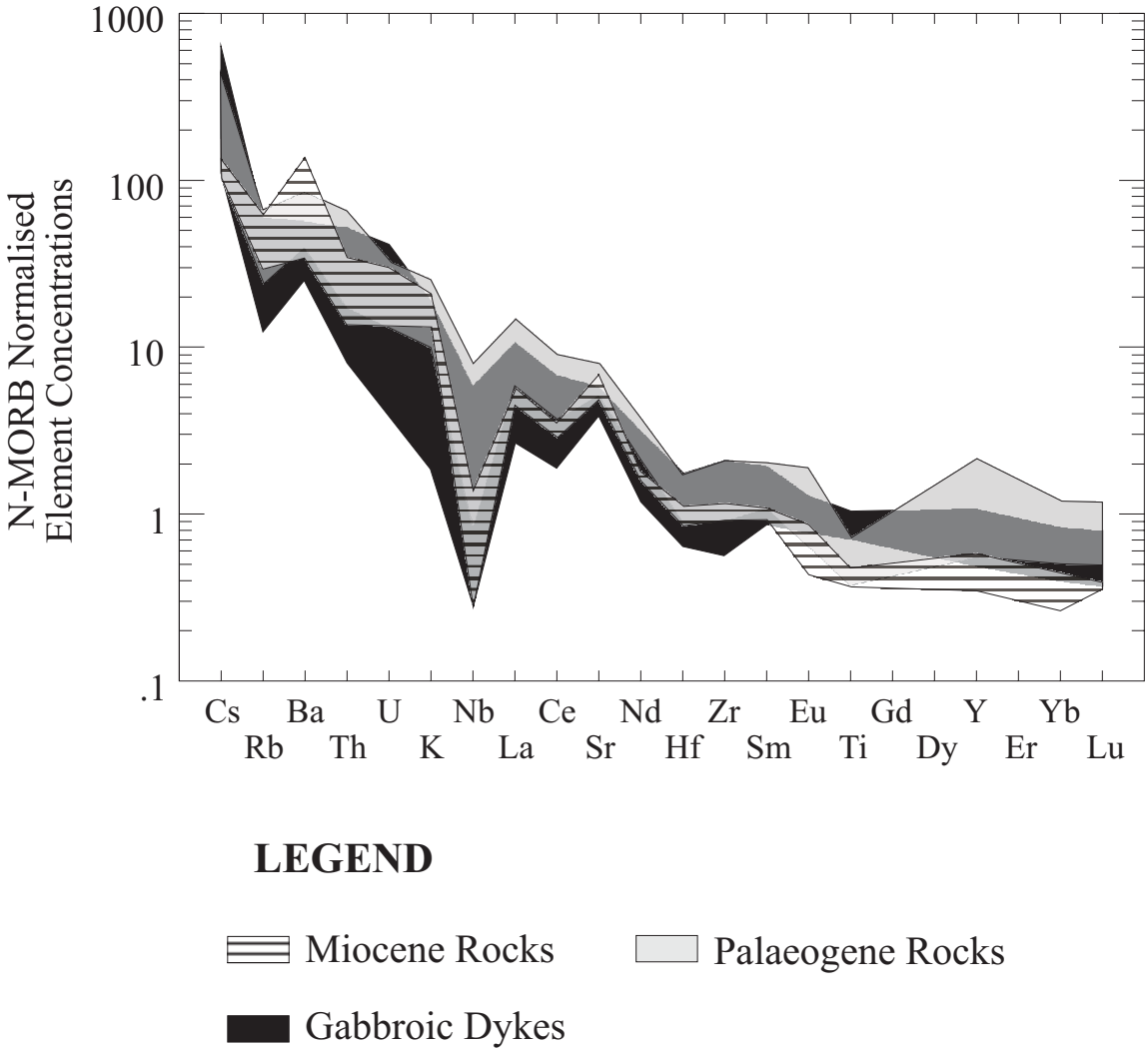

Fig. 9. N-MORB normalised incompatible trace element plots for the different rock suites. Normalising values from Sun and McDonough (1989).

C.8 Rare Earth Elements

All the igneous units display enrichment in LREE on chondrite-normalised plots (Fig. 10). The majority of samples lack an Eu anomaly, with only a few displaying weak negative Eu anomalies. A hornblende diorite dyke southeast of El Galeno (S-16) has the lowest LREE/HREE ratio, La_N/Yb_N, of 4.0, as well as the lowest total REE abundances. The Yanacocha intrusive porphyry sample has the highest La_N/Yb_N ratio at 21.8, but a sample from the Llama-Calipuy Volcanic Sequences (S-32) has the highest total REE abundances.

Gabbroic dykes sampled from the region have the flattest REE profiles (Fig. 10) with La_N/Yb_N between 4.0 and 11.0, at an average of 7.0 (Table 2). The dykes have a wide range in REE abundances and show a decrease in total REE with fractionation. Decreased La_N/Yb_N also accompanies the decrease in total REE from gabbro to hornblende diorite units. The two basic intrusive units with hornblende phenocrysts lack depletion in the middle to heavy REE.

Palaeogene felsic rocks have the highest REE abundances of all the igneous rocks. Increased REE abundances are associated with higher SiO_2 content. Palaeogene felsic units have La_N/Yb_N ranging from 5.1 to 16.1 with an average of 8.9. The intrusive samples from the Cerro Montana region have relatively flat patterns compared to the other Palaeogene samples (Fig. 10). An Eocene volcanic unit (S-21) from the Lower Llama Volcanic Formation displays a moderate depletion in the MREE to HREE compared to the other Palaeogene units.

Barren Miocene intrusive rocks display linear and steep REE profiles. They have a range in the La_N/Yb_N ratio from 7.4 to 13.3, at an average of 10.9, and show limited variation in both LREE and HREE content (Fig. 10). Synmineralisation intrusions tend to display even steeper REE trends and a slight depletion in Sm. These intrusive units have a La_N/Yb_N from 9.7 to 21.8, with the highest average of 12.9. The Yanacocha porphyry was the youngest intrusive unit sampled and has the highest La_N/Yb_N ratio (Table 2). REE profiles of samples from Miocene mineralised systems also display moderate variation in HREE content compared to the uniform LREE content. Late Miocene volcanic units display similar trends to the Miocene intrusions and have a

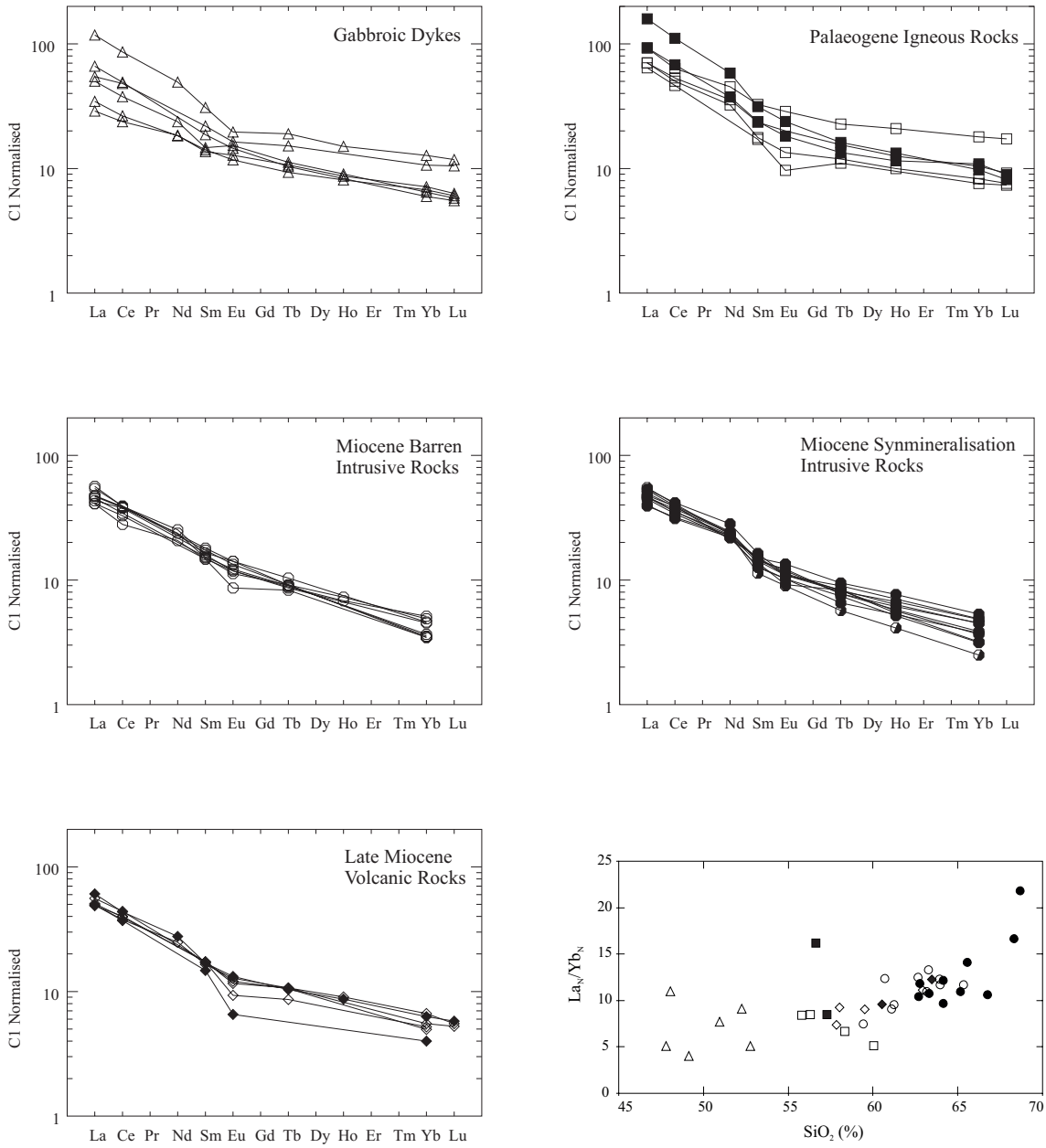

Fig. 10. Chondrite normalised REE profiles and La_N/Yb_N vs. SiO_2 plot for igneous suites in the Cajamarca region. Chondrite normalised values from Taylor and McLennan (1985).

Table 2. La_N/Yb_N ratios of igneous suites in the Cajamarca region. Chondritic values of Taylor and McLennan (1985).

Suites	**La_N/Yb_N Ratio**		
	Minimum	**Maximum**	**Average**
Suite 1 - Gabbroic Dykes	4.0	11.0	7.0
Suite 2 - Palaeogene Igneous Units	5.1	16.1	8.9
Suite 3a - Miocene Intrusive Units			
- *Barren Stocks*	7.4	13.3	10.9
- *Synmineralisation Stocks*	9.7	21.8	12.9
Suite 3b - Miocene Volcanic Units	7.4	12.3	9.8

La_N/Yb_N from 7.4 to 12.3, with an average of 9.8. Total REE for both the Regalado and Huambos formations decrease with increasing fractionation. The late Miocene volcanic samples display a slight Sm depletion and two samples (S-MC4 and S-68) also display negative Eu anomalies.

C.9 Rb-Sr and Sm-Nd Isotope Compositions

Sr and Nd isotopic compositions of selected magmatic rocks were also conducted during the study. However, several of the magmatic rocks were altered by later hydrothermal fluids. Hydrothermal fluids exsolved from a magma chamber may contain different isotopic compositions to the host intrusion (Skewes and Stern, 1996). Such variations may result from hydrothermal fluids interacting with wall rock during ascent from the magma chamber, or alternatively hydrothermal fluids may have been released from a compositionally different magma chamber. A pilot study including two samples was performed to detect any disturbances to the Sr and Nd isotopic system that resulted from the fluxing of hydrothermal fluids through the host intrusive rock. A moderately to strongly altered gabbroic dyke (S-16) and a weakly altered quartz diorite (S-59) were chosen based on degree of alteration and known age. These samples were analysed both as bulk whole rock powders and leached residual material. Leached samples were washed with hot 6M HCl prior to analysis to remove secondary carbonate material. The residual leached material is inferred to represent the original isotopic composition of the intrusive rock before hydrothermal fluxing. The results show a large amount of REE material was removed from the altered dyke (S-16) during the leaching process (Table 3). For the dyke, $^{143}Nd/^{144}Nd$ and $^{143}Sm/^{144}Nd$ ratios for the residual material are higher than the bulk powders. In contrast, the same isotopic ratios for the quartz diorite bulk powder are higher than the residual material. However, the difference in $^{143}Nd/^{144}Nd$ for both the bulk powder and residual material is minimal. Sr isotopic ratios are lower in both samples for the residual material than the bulk powder. These results suggest primary Sr, Rb and REE located along lattice edges of accessory minerals may have been removed during the leaching process, or, alternatively the majority of the REE are located in the secondary carbonate material. The large amounts of REE removed from the altered dyke suggest the latter. This indicated hydrothermal fluids have probably perturbed the original isotopic ratio for the intrusive rocks. Based

Table 3. Results from radiogenic Sr and Nd isotope analyses.

Sample no.	Sm ppm	Nd ppm	Rb ppm	Sr ppm	$(^{147}Sm/^{144}Nd)_m$	$(^{143}Nd/^{144}Nd)_m$	$\varepsilon_{Nd(0)}$	Age (Ma)	TDM (Ga)	$(^{87}Rb/^{86}Sr)_m$	$(^{87}Sr/^{86}Sr)_m$	$(^{87}Sr/^{86}Sr)_i$	Bulk weight (g)	Residue weight (g)
Palaeocene-Eocene Intrusive & Volcanic Rocks														
S-46 (Intr)	3.29	14.43	56.2	699	0.1361	0.512779	2.76	57.0	0.731	0.233	0.70422	0.70403	0.0408	0.0216
S-31 (Intr)	4.51	21.07	58.1	1246	0.1294	0.512781	2.79	47.0	0.670	0.135	0.70556	0.70547	0.0411	0.0197
S-32 (Volc)	2.95	14.89	82.5	925	0.1197	0.512814	3.44	43(?)	0.547	0.258	0.70399	0.70383	0.0414	0.0200
S-21 (Volc)	2.38	12.17	67.6	938	0.1180	0.512803	3.22	42.6	0.556	0.209	0.70483	0.70470	0.0431	0.0214
Oligocene Gabbroic Dykes														
S-16	1.12	3.74	23.4	322	0.1812	0.512751	2.20	29.4	1.870	0.211	0.70465	0.70455	0.0316	0.0212
S-57	2.54	11.24	29.9	516	0.1364	0.512742	2.03	29.4	0.808	0.168	0.70436	0.70428	0.0409	0.0186
Barren Miocene Intrusions														
S-11	1.42	5.98	59.8	559	0.1436	0.512691	1.04	21.3	1.000	0.310	0.70482	0.70473	0.0403	0.0342
S-59	1.75	8.89	62.4	392	0.1189	0.512695	1.10	20.6	0.740	0.461	0.70458	0.70445	0.0351	0.0299
S-38	1.06	6.01	80.1	784	0.1061	0.512728	1.76	17.9	0.600	0.296	0.70463	0.70456	0.0404	0.0238
S-T4	2.89	13.87	56.8	586	0.1261	0.512770	2.57	16.5	0.665	0.281	0.70478	0.70471	0.0422	0.0209
Synmineralised Early-Mid Miocene Intrusions														
S-Chail	1.21	5.65	54.9	693	0.1291	0.512715	1.50	23.2	0.787	0.229	0.70472	0.70464	0.0419	0.0303
S-H22 (176)	2.37	11.87	42.8	672	0.1205	0.512791	2.98	19.8	0.591	0.184	0.70429	0.70424	0.0431	0.0316
S-T2	0.44	2.87	53.4	530	0.0916	0.512684	0.89	17.5	0.585	0.291	0.70508	0.70501	0.0419	0.0345
Miocene Volcanic Rock														
S-MC4	1.79	8.90	75.1	632	0.1212	0.512728	1.75	9(?)	0.699	0.344	0.70472	0.70468	0.0408	0.0319
Mineralised Late Miocene Intrusion														
S-CLL5	0.92	7.60	84.4	881	0.0728	0.512667	0.56	10.0	0.525	0.278	0.70500	0.70496	0.0429	0.0357
S-11 (repeat)			64.8	622						0.302	0.70476		0.0400	0.0316
Pilot Study														
S-16 bulk	3.16	13.41	31.8	510	0.1426	0.512708	1.37		0.950	0.181	0.70474		0.0191	na
S-16 res-HCl	1.12	3.74	23.4	322	0.1812	0.512751	2.20		1.870	0.211	0.70465		0.0316	0.0212
S-59 bulk	3.32	15.87	57.4	1288	0.1264	0.512729	1.80		0.740	0.129	0.70512		0.0224	na
S-59 res-HCl	1.75	8.89	62.4	392	0.1189	0.512695	1.10		0.740	0.461	0.70458		0.0351	0.0299

all $^{143}Nd/^{144}Nd$ are relative to La Jolla-Nd = 0.511860; all $^{87}Sr/^{86}Sr$ are relative to SRM987-Sr = 0.71024

$\varepsilon_{Nd(0)}$ calculated for present-day CHUR = 0.512638

m = measured; *i* = initial; TDM - Depleted Mantle Age; na = not analysed

Bulk weight - weight of whole rock powder; Residual weight - weight of residual material after leaching

on these results, the remaining 13 samples analysed were leached in hot 6M HCl to remove any secondary material that may have resulted in a bias related to hydrothermal fluxing of the host intrusive rock. This was considered to deliver the most accurate determination for the original primary isotopic ratio.

Igneous rocks from the Cajamarca district display a broad array of both initial $^{87}Sr/^{86}Sr$ (Sr_i) values that range between 0.7038 and 0.7055, and epsilon Nd [$\varepsilon_{Nd(0)}$] that range from +3.44 to +0.56 (Table 3, Fig. 11). The samples display an overall change from high $\varepsilon_{Nd(0)}$ and low Sr_i, through to high Sr_i and low ε_{Nd}. The Palaeogene magmas have higher $\varepsilon_{Nd(0)}$ values (+3.44 to +2.76) and a larger range of Sr_i (0.7038-0.7055) than the younger Miocene igneous units. The Cerro Montana sample (S-31) has anomalously high Sr_i but similar $\varepsilon_{Nd(0)}$ values to the other Palaeogene units. The gabbroic dykes have Sr_i ranging from 0.7043 to 0.7046 and lower $\varepsilon_{Nd(0)}$ values than the Palaeogene felsic rocks. Barren intrusive units have Sr_i between 0.7045 and 0.7047, with $\varepsilon_{Nd(0)}$ values that increase with age from +2.57 to +1.04. The mineralised centres have large $\varepsilon_{Nd(0)}$ and Sr_i ranges ($\varepsilon_{Nd(0)}$ = +2.98 to +0.56; Sr_i = 0.7043-0.7050), which overlap with coeval barren intrusions. However, the isotopic compositions of a synmineralisation stock from Michiquillay ($\varepsilon_{Nd(0)}$ = +2.98; Sr_i = 0.7042) and a post-mineralisation magmatic breccia at El Galeno ($\varepsilon_{Nd(0)}$ = +2.57; Sr_i = 0.7047) are considerably more primitive with more radiogenic Nd than intrusive units of similar or slightly older age. The late Miocene volcanic rock has $\varepsilon_{Nd(0)}$ of +1.75 and Sr_i of 0.70468.

Sr_i for the gabbroic units decreases with increasing silica, whereas the Palaeogene felsic rocks show a steep positive trend. The Miocene igneous units display a slight increase in Sr_i with fractionation. A plot of $\varepsilon_{Nd(0)}$ vs. SiO_2 shows a negative correlation between $\varepsilon_{Nd(0)}$ and increasing SiO_2 content for all of the igneous units. Sr_i vs. age displays an overall increase in Sr_i with time. In contrast, $\varepsilon_{Nd(0)}$ vs. age illustrates a general decrease in radiogenic Nd with time. However, the two Miocene intrusions with primitive compositions (S-H22 and S-T4) contain elevated Nd values compared to coeval intrusions.

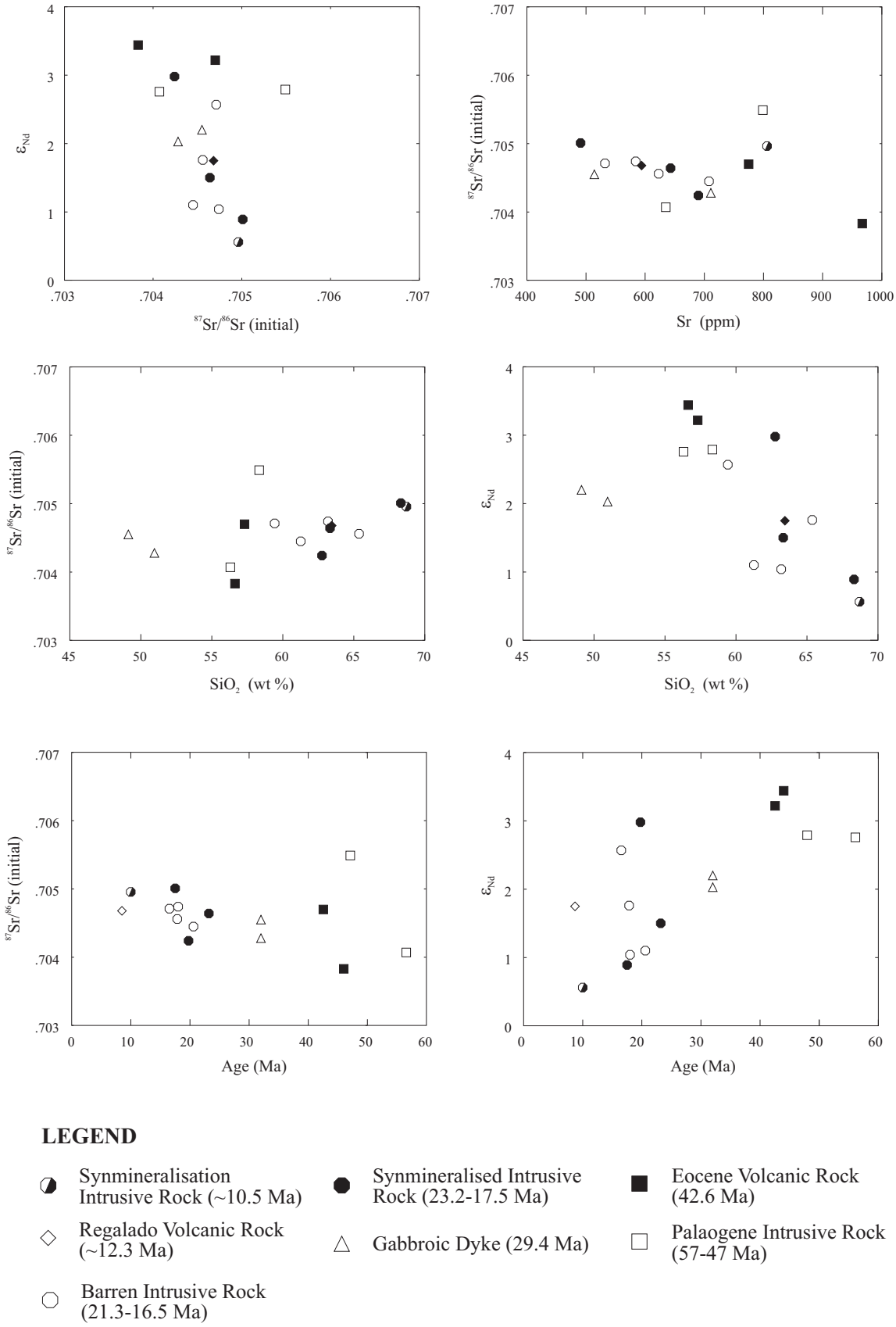

Fig. 11. Radiogenic isotope plots for selected igneous rocks from the Cajamarca region.

C.10 Petrogenetic Modelling of the Cajamarca Igneous Units

C.10.1 REE Partial Melting Models

Chondrite-normalised REE profiles of igneous units from a range of magmatic compositions have previously been modelled using partial melting, fractional crystallisation and assimilation-fractional crystallisation calculations (e.g. Petford and Atherton, 1996; Lang and Titley, 1998; Caffe *et al*., 2002). Macfarlane (1999) documented the isotopic homogeneity of Miocene igneous rocks from the Hualgayoc region and concluded the magmas represent upper sub-Andean mantle or lower sub-Andean crust melts that assimilated limited shallow crust material. Macfarlane (1999) suggested the rocks were isotopically homogenised prior to emplacement. Igneous rocks that have undergone minimal upper crustal contamination closely represent the geochemistry of their source regions. Most Miocene igneous rocks from the Cajamarca are compositionally similar to units from the Hualgayoc region (Fig. 5 in Macfarlane, 1999) and are also inferred to have undergone minimal contamination. Therefore, these rocks can be used to model source regions and possible subsequent fractional crystallisation processes. An attempt has been made to model some rocks from the Cajamarca region that are inferred to best represent unaltered and uncontaminated (low Sr_i) magmas for each of the igneous suites.

Trace element modelling presented in this paper involves two main stages, namely: (1) modelling the generation of a parent melt by partial melting of a mafic mantle source, and (2) modelling subsequent batch melting of the parent melt modelled in stage 1. Wood and Fraser (1976) defined batch melting as "continuous re-equilibration of melt with residual solid phases throughout partial melting until removal of melt". Modal mantle- and batch-melting calculations of REE, Rb, Sr, Zr and Y have been modelled for selected magmatic units. Magmatic units were chosen based on age, suite type and observed geochemistry. Batch melting models were calculated using the equation of Shaw (1970):

$$C_m = C_i / [K_D + F_m * (1-K_D)]$$

Where C_m is the trace element concentration in the partial melt, C_i is the initial trace element concentration in the source, K_D is the bulk partition coefficient and F_m is the melt fraction. No studies to date have produced a set of internally consistent partition coefficients for all minerals coexisting with a single melt. Therefore, partition coefficients used for this study (Appendix C3) were adopted from Martin (1987), who modelled partial melting of tholeiitic basalt for the generation of tonalites and granodiorites.

Stage 1 – Generation of a primitive/parent mafic melt

For modelling of a parental melt, an Oligocene hornblende gabbro (S-16) that has the lowest concentrations of SiO_2, Rb and total REE abundances, as well as a relatively low La_N/Yb_N ratio (~4) has been used to represent a primitive/parent composition for magmas found in the Cajamarca region. Primitive mantle values from McDonough *et al*. (1992) have been used to represent the source composition.

Modal mantle-melting calculations indicate a melt of similar composition to the sample S-16 can be modelled by between 4 to 7% partial melting of a primitive mantle source (Table 4; Fig. 12). The modelled residue was dominated by >50% olivine, with subordinate amounts of orthopyroxene, clinopyroxene, amphibole and garnet. Whilst the deduced REE values are consistent with analytical values, the modelled LIL and Zr contents are significantly lower than the analytical results. Elevated concentrations of LIL might occur in gabbroic differentiates derived from a feldspar depleted upper mantle-lower crust due to their compatibility with feldspar.

Stage 2 – Generation of felsic melts

The primitive melt generated in stage 1 is now used as the source to model Palaeogene and Miocene melts.

Palaeogene Magmatism

Palaeogene intrusive and volcanic rocks have high REE abundances and flat REE profiles. Sample S-46 is a microdiorite with a low Sr_i that suggests minimal crustal

Table 4. Table showing whole rock geochemistry against modelled partial melt compositions.

	Mantle Melting		Batch Melting Models									
Suite	Oligocene Dyke		Paleocene Intrusion		Early-Mid Miocene Intrusions				Miocene Volcanic Rock		Late Miocene Intrusion	
Elements	Sample 16		Sample 46		Sample Chail		Sample 59		Sample 61		Yanacocha	
	Analytical Results	5% Melt	Analytical Results	40% Melt	Analytical Results	50% Melt	Analytical Results	55% Melt	Analytical Results	50% Melt	Analytical Results	45% Melt
Rb	35	9	62	60	72	55	60	56	33	60	83	67
Sr	514	229	635	633	643	645	708	705	838	734	805	881
Zr	51	31	86	90	93	76	81	71	83	75	94	75
Y	19	20	21	28	13	14	15	15	18	20	7	8
La	10.60	10.31	25.90	23.85	19.30	19.05	17.20	17.33	18.20	18.65	20.20	20.13
Ce	22.70	23.84	48.00	47.94	37.70	37.79	36.40	34.77	36.10	36.93	39.00	39.51
Nd	13.10	11.90	23.00	23.64	17.40	17.01	16.90	16.57	17.60	17.12	16.50	17.32
Sm	3.15	3.22	4.09	5.00	3.28	3.49	3.49	3.47	3.81	3.57	2.62	3.33
Eu	1.11	1.07	1.17	1.18	0.95	0.99	0.98	1.11	1.11	1.12	0.78	1.11
Tb	0.62	0.55	0.69	0.80	0.47	0.48	0.53	0.50	0.62	0.56	0.33	0.34
Yb	1.77	1.71	2.05	2.08	1.20	1.20	1.21	1.21	1.65	1.62	0.62	0.59
Lu	0.24	0.24	0.29	0.29	-0.20	0.17	-0.20	0.17	0.21	0.23	-0.20	0.08
La_N/Yb_N	4.05	4.07	8.45	7.67	10.75	10.61	9.51	9.59	7.38	7.72	21.79	22.68
Modelled Residual Mineralogy												
Olivine		55		15		-		-		-		-
Orthopyroxene		23		20		-		-		-		-
Clinopyroxene		15		42		36		50		55		30
Garnet		3		1.5		4		5		1		17
Amphibole		4		10		50		40		38		50
K-Feldspar		-		11		7		3		3		-
Ilmenite		-		-		2		1		2		2
Magnetite		-		-		1		1		1		1

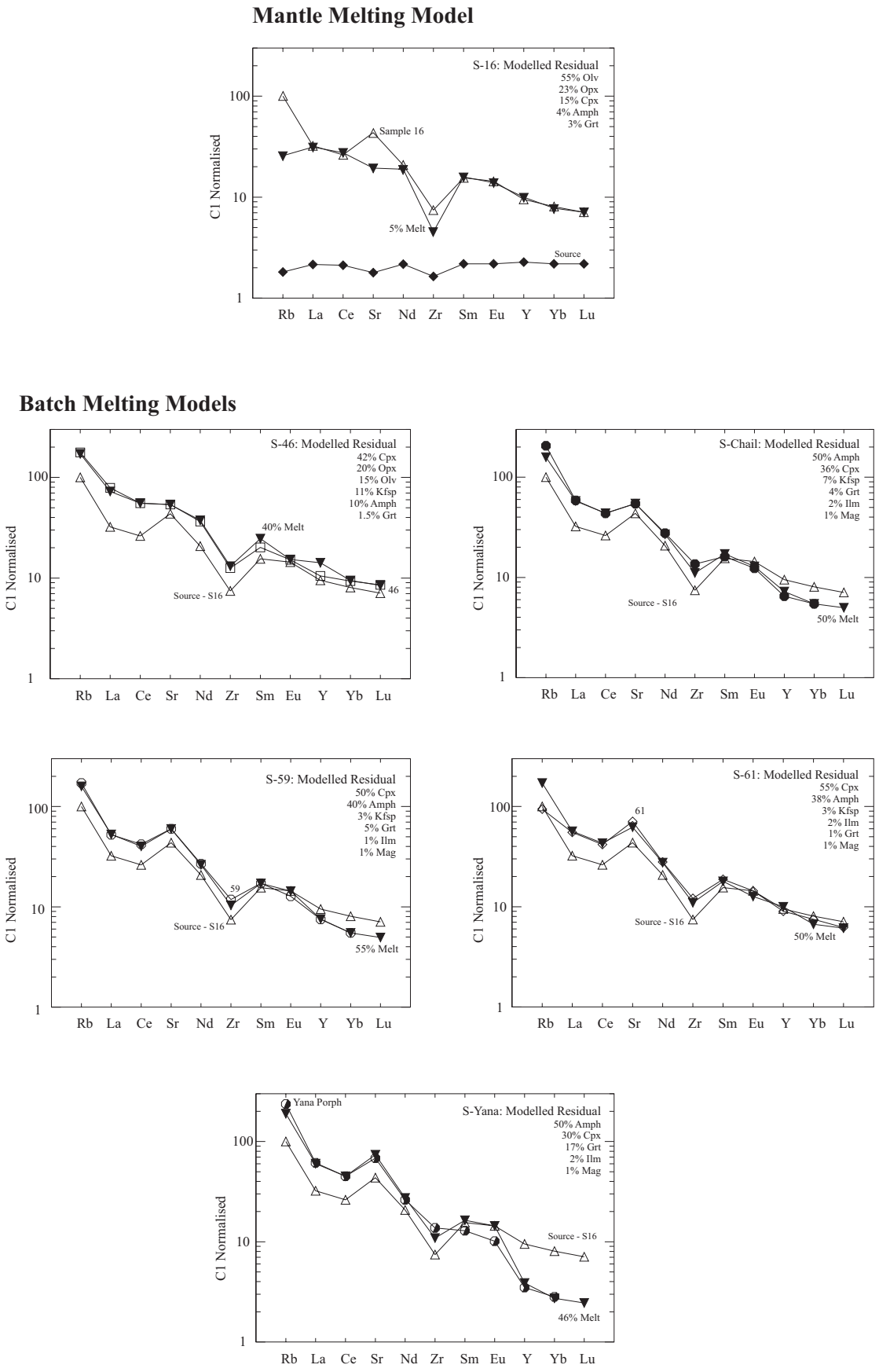

Fig. 12. Partial melting models for the different igneous suites in the Cajamarca region of northern Peru. Partition coefficient values are from Martin (1987).

contamination. This intrusion is the oldest igneous rock dated in the region at 57 Ma and is interpreted to be the most primitive and least contaminated of the Palaeogene felsic rocks. This sample is therefore used as the baseline melt composition for Palaeogene magmatic activity.

Batch-melting calculations for sample S-46 produced a dry residue composed of pyroxene, olivine, K-feldspar, minor amphibole and possibly garnet (Table 4, Fig. 12). Partial melting calculations suggest melt compositions related to development of Palaeogene magmatic units were strongly influenced by the presence of clinopyroxene compared to the olivine-dominated residue for the gabbroic dykes. Alternatively, Palaeogene units may have been derived from a different parental material or source region.

Early-Middle Miocene Magmatism

Early to middle Miocene intrusive units are predominantly diorites to quartz diorites that have moderately steep REE patterns. Barren and mineralised Miocene intrusions are both modelled. The oldest Miocene intrusion is a synmineralisation hornblende-biotite diorite (Chail) from the Minas Conga prospect at 23.2 Ma (Llosa *et al*., 1996). The barren Miocene intrusion (S-59) is slightly younger at 20.6 Ma (Section A) and can be modelled by high degrees of partial melting (~55% melt) with residues dominated by clinopyroxene, amphibole, plus minor garnet and K-feldspar (Table 4, Fig. 12). Modelled residue for the synmineralisation intrusion (Chail) has more amphibole and K-feldspar, but less clinopyroxene and garnet.

Late Miocene Magmatism

Miocene volcanic rocks show a wide range in SiO_2 and display flat to moderately steep REE patterns. This change from flat to steep trends is also accompanied by a progressive change in the modal mineralogy that probably reflects fractional crystallisation in shallow level magma chambers. Regalado volcanic rocks, of late Miocene age (12 Ma, Turner, 1997), can be modelled from a garnet-poor residue containing amphibole, clinopyroxene and K-feldspar (Table 4, Fig. 12). This modelled residual is very similar to that modelled for the early to middle Miocene intrusions.

The Yanacocha porphyritic intrusion (~10 Ma) has the steepest REE pattern of all the igneous units sampled in the region. It has strong depletion in HREE and can be modelled by ~45% melting of the parent mafic material. The modelled residue consists dominantly of amphibole with subordinate garnet, clinopyroxene and K-feldspar (Table 4). The modelled REE profile also displays a positive Eu anomaly in contrast with the observed REE pattern. The difference in Eu content between the modelled and observed trend may be explained through shallow-level fractionation of plagioclase. Similar changes in Eu anomalies have been observed and modelled at numerous porphyry copper complexes, such as Santa Rosa, Peru (Le Bel, 1985), Wushan, China (Zhitian and Kezhang, 1989), as well as in the Ray and Christmas Districts, Arizona (Lang and Titley, 1998). This model requires significantly higher residual garnet compared to the Miocene volcanic rocks suggesting a rapid change in the physical conditions of the source region, different source regions or that the rocks are of different age.

C.10.2 Sm vs. Th Bivariate Plot

Fractionation Trends

A Sm vs. Th log-log bivariate plot has been used to determine variations in trace element partitioning for the different igneous rock units sampled in the Cajamarca region. Th is highly incompatible throughout differentiation and generally immobile during hydrothermal processes (Kerrich and Wyman, 1997). Therefore, Th will be used as a fractionation index. Sm has a higher K_D value for amphibole/liquid compared with pyroxene/liquid thus highlighting differences between hydrous and anhydrous crystallisation assemblages (Aldanmaz *et al*., 2000). The Sm K_D value for amphibole increases with increasing fractionation (from basic to acidic melt compositions), thereby further highlighting magma compositions controlled by the fractionation of amphibole. Sm and Th K_D values for andesitic melt compositions have been adapted from Gill (1981), Green and Pearson (1985), and Nash and Creecraft (1985) to generate theoretical Rayleigh vectors (Appendix C4).

Samples of varying ages plot along different trends on a log Sm vs. log Th plot of igneous rocks from the Cajamarca region (Fig. 13). Gabbroic dykes display a linear

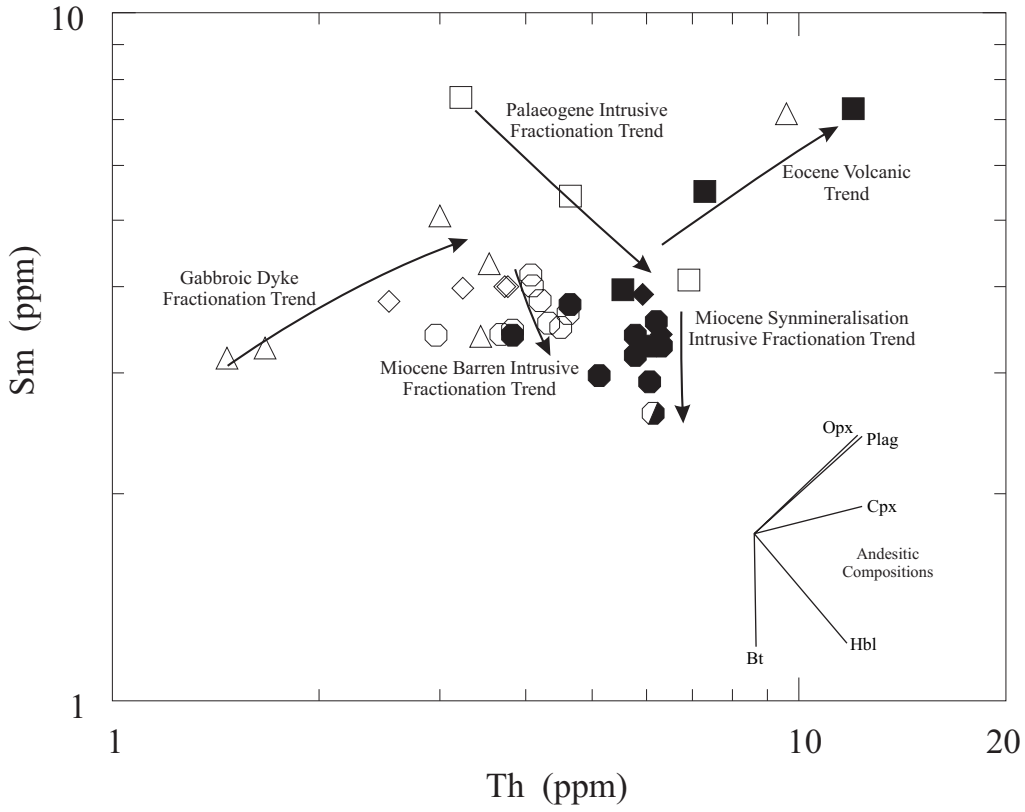

Fig. 13. Log Th vs. log Sm diagram showing theoretical Rayleigh vectors modelled for fractional crystallisation trends of an andestic melt. Partition coefficients for the fractionation model are from Gill (1981), Sm in hornblende from Green and Pearson (1985) and biotite for acidic magmas from Nash and Creecraft (1985).

increase in Sm with Th. Theoretical Rayleigh vectors suggest the compositions of these rocks were dominantly controlled by the fractionation of anhydrous minerals, such as plagioclase, orthopyroxene and clinopyroxene. Palaeocene-Eocene intrusive samples decrease in Sm with increasing Th. Significantly, Th decreases with increasing SiO_2 for these samples (Fig. 8) possibly suggesting Th saturation. Therefore, inferred hornblende fractionation from the theoretical vector trend is not applicable. In contrast, Sm and Th in Eocene volcanic samples display a positive correlation, suggesting an anhydrous mineral-dominated fractionation trend.

Miocene intrusive rocks show a general decrease in Sm with increasing Th. The barren Miocene intrusions display similar but slightly steeper trend than the Palaeocene intrusions indicating strong hornblende and minor biotite fractionation. Synmineralisation samples show minimal variation in Th with decreasing Sm. Theoretical Rayleigh vectors combined with petrographic evidence indicate melt compositions of Miocene synmineralisation stocks were strongly influenced by biotite and minor hornblende fractionation. In contrast, Miocene volcanic rocks tend to display a flat trend with minimal variation of Sm content with increasing Th. This suggests melt composition for the Miocene volcanic sequences was controlled by the fractionation of both hydrous and anhydrous minerals.

C.11 Discussion

C.11.1 Geochemistry of the Cajamarca Igneous Rocks

Petrographic and geochemical features have been used to characterise three igneous suites in the Cajamarca region; these include (1) gabbroic dykes, (2) Palaeogene felsic and (3) Miocene igneous rocks. All three suites are depleted in HFSE relative to LILE and LREE, a characteristic of subduction-related magmas that is considered to result from metasomatism of the source by LILE-rich hydrous fluids or a residual HFSE-bearing phase such as Ti-phases or amphibole (Pearce, 1983; Hawkesworth *et al*., 1993; Thirlwall *et al*., 1994).

The gabbroic dykes are tholeiitic with compositional trends that suggest clinopyroxene and possibly olivine fractionation. The dykes display primitive arc

characteristics with increasing Zr, Y, REE content with increasing SiO_2 (Pearce and Norry, 1979). With the exception of two samples that contain hornblende phenocrysts, most gabbroic dykes contain anhydrous mineral assemblages. At shallow depths outside the stability field of amphibole, fractionation of basaltic melts will be dominantly controlled by anhydrous mineral assemblages (e.g. plagioclase, orthopyroxene, clinopyroxene and magnetite) and follow tholeiitic lines of descent (Wilson, 1989). Palaeogene felsic units display similar major and trace element trends to the gabbroic dykes. Palaeogene rocks increase in Al_2O_3, MnO, P_2O_5, Zr, Y and REE contents with fractionation. These trends suggest Zr and P were incompatible. Palaeogene units also display a decrease in Th content with increasing SiO_2. Trace element models suggest anhydrous and possibly hydrous mineral fractionation occurred. In comparison, Miocene igneous units display negative correlations between Na_2O, P_2O_5, Sr and LREE with SiO_2. Samples from mineralised Miocene intrusive complexes are enriched in K_2O and Th, and depleted in Ba, compared to barren intrusive units of similar age. The mobility of K_2O and Ba during hydrothermal alteration (Kerrich and Wyman, 1997) possibly explains variations of these elements. Miocene volcanic rocks display similar trends to the Miocene intrusions but some rocks have negative Eu anomalies. Major and trace (including rare earth) element data of Miocene igneous rocks suggest both hydrous and anhydrous mineral fractionation. These fractionation processes took place outside the stability field of plagioclase for all of the Miocene intrusive and most of the volcanic rocks.

C.11.2 Source Interpretation

Petrogenetic models for arc magmas developed prior to intensive crustal thickening suggest olivine-pyroxene-oxide mineral phases controlled fractionation near the base of the crust (Atherton *et al*., 1985; Hildreth and Moorbath, 1988). Rare earth element partial melt modelling suggests Palaeogene melts equilibrated with anhydrous mineral phases (i.e. pyroxene and olivine) and an amphibole- and garnet-poor residue. Palaeogene felsic and Oligocene mafic igneous rocks from the Cajamarca region display a large variation in Sr_i (0.7038-0.7055) across a narrow silica and ε_{Nd} range. Th displays a steep negative correlation with increasing SiO2 possibly suggesting Th saturation or upper crustal contamination (Richards and Villeneuve, 2002). Isotope compositions suggest a low radiogenic Nd - high radiogenic Sr, possibly such as

seawater or upper crustal, contaminated the source region of some Palaeogene magmas. Radiogenic isotope ratios and partial melting models suggest these melts were derived from a young magmatic arc environment in which the base of the crust was shallower than at present, and dominated by olivine and pyroxene mineral residues.

Atherton *et al*. (1985) concluded that the Eocene Calipuy volcanic rocks in northern Peru were derived from partial melting of garnet-free peridotite mantle and underwent later fractionation of anhydrous minerals. Trace element models of Palaeogene magmas indicate anhydrous mineral assemblages (plagioclase and pyroxene) controlled fractionation of the volcanic melts, whereas intrusive melts follow hornblende fractionation trends. This suggests intrusive melt compositions were characterised by slightly higher magmatic water.

The Cajamarca and Hualgayoc igneous rocks have higher Sr_i than Cretaceous igneous rocks of the northern Coastal batholith (on average 0.7040-0.7043; Beckinsale *et al*., 1985) but lower Sr_i values than younger Miocene intrusive units from the Cordillera Blanca Batholith (0.7041-0.7057; Petford *et al*. 1996). Such increases in radiogenic Sr with time are observed throughout the entire Andean belt and inferred to be the result of increased crustal contamination due to thickening of the crust (Davidson *et al*., 1991) or variations in the source (Petford *et al*., 1996). Macfarlane (1999) documented the isotopic homogeneity (Pb, Nd and Sr) of igneous rocks and ores from the Hualgayoc district concluding that the isotope data supported a model of subducted sediment enriching the mantle wedge to generate the parental magmas. Such a model does not require assimilation and contamination of the Cretaceous sedimentary rocks or metamorphic basement. Miocene igneous rocks from both the Cajamarca and Hualgayoc regions have similar isotopic compositions (Fig. 14). Miocene igneous units from Cajamarca (0.7043-0.7050) and Hualgayoc (0.7043–0.7048; Macfarlane, 1999) have overlapping Sr_i compositions (Fig. 14), although most rocks from the Cajamarca contain slightly more radiogenic Nd. The Miocene rocks from both regions display a slight increase in Sr_i with time. Two samples from mineralised centres in the Cajamarca region (H-22 – synmineralisation; T4 – post-mineralisation) and a dioritic dyke from the Hualgayoc region have primitive isotopic compositions compared to intrusions of similar or older age. These primitive compositions possibly reflect replenishment of the mantle or magma chamber with new parental mafic melts. Isotopic compositions of

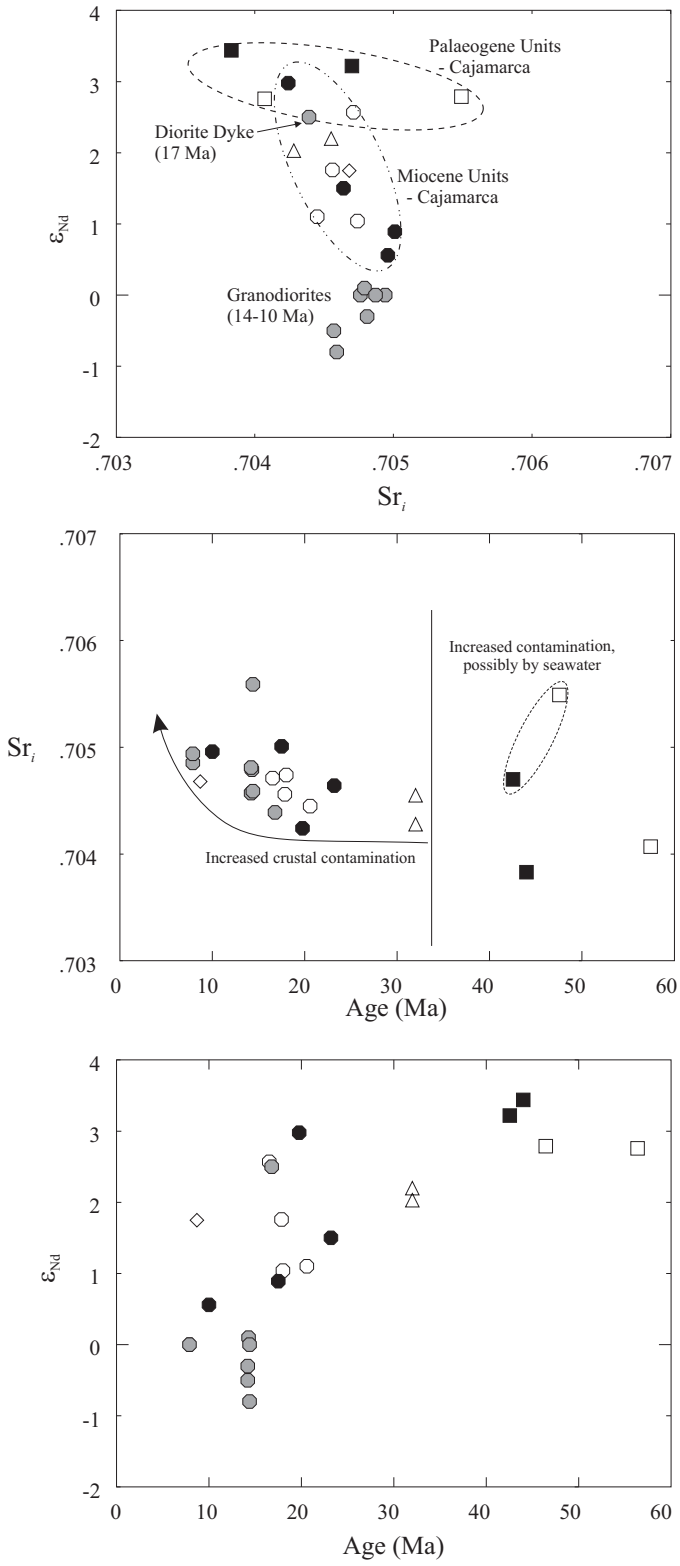

Fig. 14. ε_{Nd} and Sr_i plots showing isotopic values for magmatic rocks from the Cajamarca and Hualgayoc district (Macfarlane, 1999).

Miocene igneous rocks from the Cajamarca and Hualgayoc regions indicate these magmas were derived from an enriched mantle that homogenised at deep levels, possibly in the upper mantle, and underwent minimal assimilation or contamination.

Based on outcrop evidence, early to middle Miocene times in the Cajamarca region were characterised by the emplacement of numerous intrusive stocks and were followed by extensive late Miocene volcanic activity. Miocene igneous rocks show a general depletion in both middle and heavy rare earth elements with increasing silica content. Some of the late Miocene volcanic rocks have a slight Eu anomaly, whereas the majority of Miocene intrusions lack negative Eu anomalies. The absence of a negative Eu anomaly may result from high magmatic oxidation states and/or suppression of plagioclase fractionation (e.g. Frey *et al*., 1978; Lopez, 1982; Lang and Titley, 1998). Magmatic trends for rocks of intermediate to acidic composition, such as observed in the Miocene igneous units, are commonly attributed to the increasing abundance of residual garnet in the source (Arth *et al*., 1978; Kay *et al*., 1991; Petford and Atherton, 1996; Kay and Mpodozis, 2001), and/or the fractionation of hornblende (Lang and Titley, 1998; Aldanmaz *et al*., 2000). Partial melting models suggest Miocene magmas were derived from an amphibole-rich residue but garnet content increased with time. This interpretation is supported by xenoliths in tuffs from SW Columbia that indicate hornblende-bearing assemblages dominate the deep crust of the northern Andes (Weber *et al*., 2002). The modelled amphibole-rich assemblage contrasts with the deduced Palaeogene olivine-pyroxene-rich residue (Fig. 15a). This major change in residual mineralogy coincided with intense crustal thickening in northern Peru, possibly indicating partial melting occurred at depths similar to those observed today, i.e. ~45 km (Fukao *et al*., 1989), and at greater temperature-pressure regimes to Palaeogene times. Trace element models also indicate that fractionation of hydrous minerals (e.g. hornblende and biotite) controlled melt compositions of the Miocene intrusions. In contrast, clinopyroxene and plagioclase fractionation influenced the composition of late Miocene volcanic rocks.

C.11.3 Model for Porphyry Cu Formation

Kay and Mpodozis (2001) proposed a three-stage model for generation of magmas related to the formation of giant Miocene Andean ore deposits in Chile. This

Fig. 15. Schematic magmatic and tectonic reconstruction of a section through the northern Peruvian Andes and Cajamarca region from Eocene to late Miocene times. (A) Eocene magmas are characterised by an olivine-pyroxene residual mineralogy, intruded the metamorphic basement and deformed Cretaceous sedimentary rocks and host no known mineralisation. (B) Early-middle Miocene magmas developed beneath a thickened crust, equilibrated with a wet amphibole-rich residue and are associated with a number of porphyry Cu deposits. Barren Miocene stocks underwent hornblende fractionation, whereas the composition of coeval synmineralisation stocks was controlled by biotite fractionation. (C) Formation of late Miocene high-sulphidation deposits occurred during termination of crustal thickening and onset of a flattening of the subduction zone. Late Miocene magmas equilibrated with a residual mineralogy that contained a higher garnet content than earlier magmas.

(a) Eocene Magmatism (57-43 Ma)

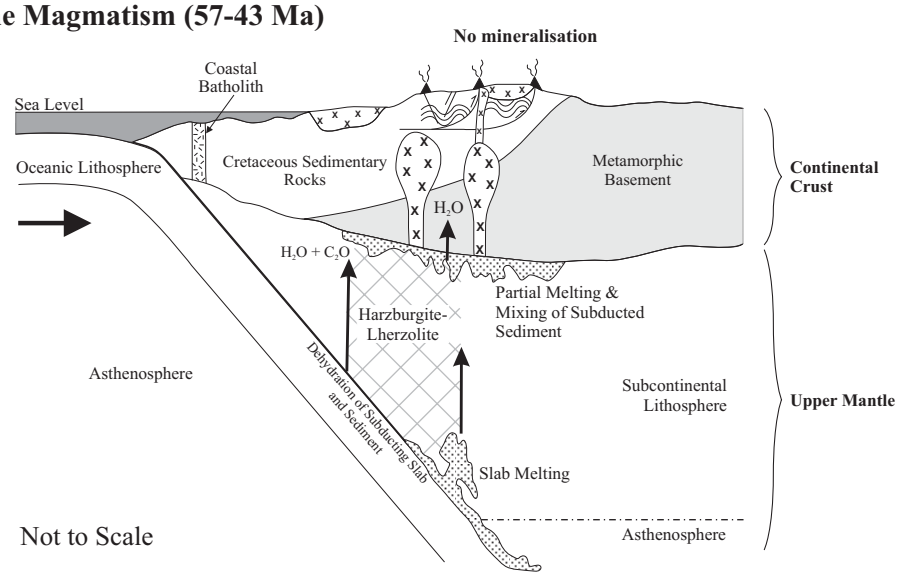

(b) Early-Mid Miocene Magmatism (23-17 Ma)

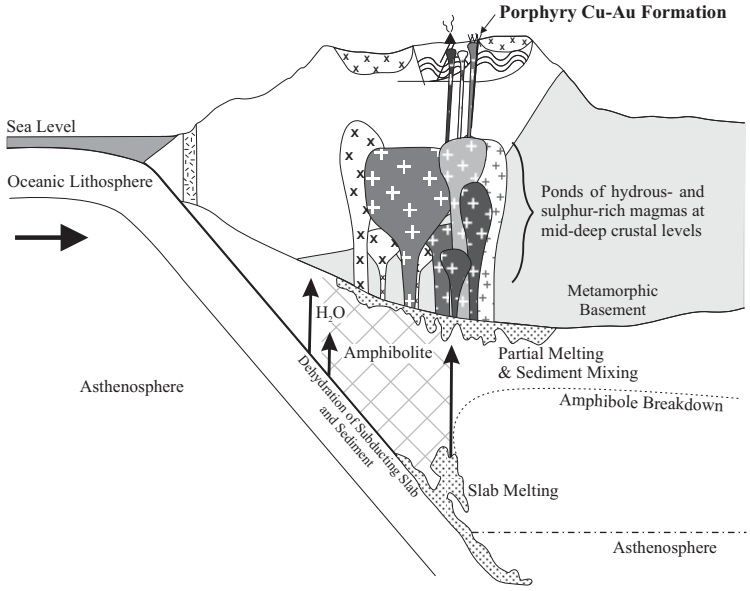

(c) Late Miocene Magmatism (~11 Ma)

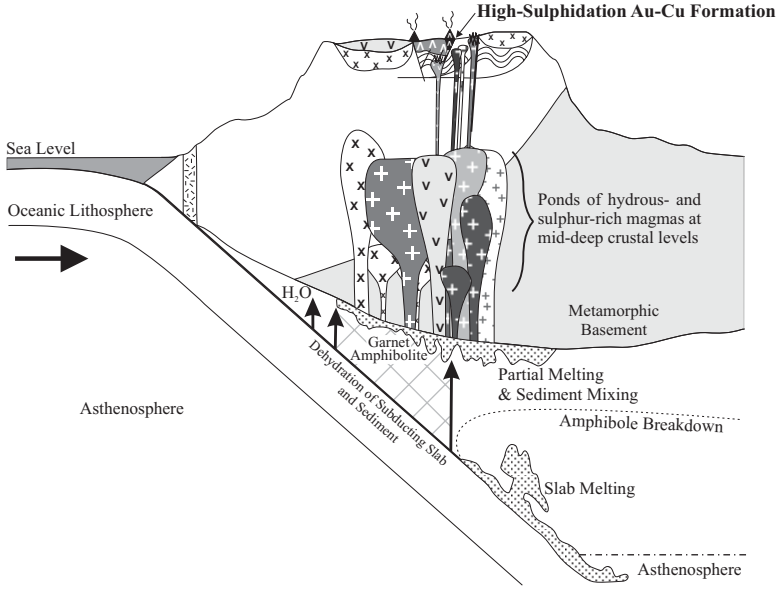

model incorporates shallowing of the subduction zone beneath a thickening crust and a progressive change from pyroxene- to amphibole- and finally garnet-bearing mineral residues. Large amounts of fluids released during the breakdown of the amphibole-bearing source resulted in development of hydrous oxidised melts. Storage of these hydrous melt at the lithosphere-crust interface in a compressive tectonic regime could have promoted fractional crystallisation, crustal contamination and melting-assimilation-storage-homogenisation (MASH) processes as outlined by Hildreth and Moorbath (1988). Generation and homogenisation of hydrous melts beneath a thickening crustal have been proposed as influential processes for the formation of porphyry copper deposits in Chile (Campos *et al*., 2002; Richards *et al*., 2001, Kay and Mpodozis, 2001; Oyarzun *et al*., 2001).

Geochemical and petrological data from the Cajamarca region suggest a different mode of porphyry Cu formation to that proposed in northern Chile. Porphyry Cu deposits in the Cajamarca region are inferred to have formed as a result of the following processes. Dehydration of the subducted slab released H_2O-rich fluids from the breakdown of hydrous minerals (e.g. Na-amphibole, lawsonite, chlorite) and caused decarbonation of subducted pelagic sediment, large-scale hydration of the lithospheric wedge and generated large volumes of partial melt (c.f. Peacock, 1993; Peacock *et al*., 1994). Experimental studies suggest silica and incompatible elements would also have been removed from both the subducted slab and sediments, and would then have ascended with H_2O-rich fluids to enrich the mantle wedge (Nakamura and Kushiro, 1974; Stern and Wyllie, 1978). These wet fluids induced development of parental mafic melts and supported continued crystallisation of hydrous mineral phases, in particular amphibole, in the mantle (Peacock, 1993). These primitive mafic melts may have undergone differentiation and possibly assimilation-fractional crystallisation (AFC) or MASH-type processes in an amphibole-rich upper mantle to lower crust interface. However, these later processes do not appear to have significantly influenced the generation of synmineralisation magmas in the Cajamarca district. Such processes are likely to occur during compressional regimes and beneath a thickened crust where melts preferentially pond and evolve at depth rather than migrate upwards into the mid or upper crust (Davidson *et al*., 1991; Campos *et al*., 2002).

Clusters of porphyry Cu deposits in Chile overlie large-scale magnetic anomalies that Behn *et al*. (2001) have interpreted as deep mafic to intermediate parental intrusive bodies of batholithic size. Highly oxidised, water-rich mafic melts have high sulphur solubility and are effective carries of chalcophile elements (Burnham, 1979). The content of sulphur and chalcophile elements in mafic melts is likely to increase with increased partial melting in the upper mantle (Burnham, 1981). Repeated injection of primitive hydrous melts into mid to deep crustal level magma chambers would further increase the concentration of sulphur.

During stages of high magmatic water content (in excess of 4 wt % H_2O) hornblende fractionation and suppression of plagioclase crystallisation may also occur, and result in segregation of hornblende (Naney, 1983: Merzbacher and Eggler, 1984; Rutherford and Devine, 1988). Continued fractionation and segregation of hornblende lowers the CaO, MREE-HREE and magmatic H_2O content in the melt. If the CaO content drops below the level required for amphibole crystallisation, biotite will replace hornblende as the dominant cotectic mafic phase (Naney, 1983; Candela, 1997; Richards *et al*., 2001). Such a change from hornblende- to biotite-dominated fractionation is observed between barren and synmineralisation stocks in the Cajamarca region and deposits in northern Chile (Richards *et al*., 2001). Oyarzun *et al*. (2001) proposed that giant porphyry Cu deposits in Chile are associated with hydrous melts that retained high sulphur levels and were emplaced in the upper crust during a low volcanic/intrusive ratio period as “closed or near-closed porphyry system”. Such systems have the potential to generate large concentrations of sulphides during plutonic crystallisation and hydrothermal processes.

As the water content in the mantle declined to due the breakdown of hydrous minerals, such as amphiboles and micas, high temperature/pressure anhydrous mineral phases crystallised (e.g. garnet and clinopyroxene). Kay and Mpodozis (2001) suggested that major Miocene ore deposits in Chile formed during progressive flattening of the subducting slab, which coincided with a change in the residual mineralogy from amphibole- to garnet-dominated They further argued the potential for significant mineralisation decreases as a dry, garnet-dominated source evolves. Trace element models of Miocene igneous rocks in the Cajamarca district suggest porphyry Cu-Au-Mo mineralisation occurred during the transition from a garnet-poor amphibole-

dominated residue (50% amphibole, 5% garnet) in the early Miocene to an amphibole-garnet residue (50% amphibole, 17% garnet) during the late Miocene (Fig. 15b). The increasing presence of garnet as a residual mineral is linked to the cessation of crustal thickening (Noble *et al*., 1990) and the onset of a flattening subduction angle in northern Peru approximately 12 to 10 Ma (Gutscher *et al*., 1999). Formation of high-sulphidation Au deposits in the late Miocene were therefore temporally linked to flattening of the subduction angle, cessation of crustal thickening and a further change in residual mineralogy (Fig. 15c).

C.12 Conclusion

Porphyry Cu and high-sulphidation Au deposits in the Cajamarca region formed during early-middle Miocene and late Miocene magmatic events, respectively. Synmineralisation stocks are geochemically similar from coeval barren intrusions, but both differ significantly from barren Palaeogene magmatic rocks. Miocene mineralisation resulted from the culmination of progressive changes in the tectonomagmatic setting of the Cajamarca region during Tertiary times. The following features have important implications for Tertiary arc magmatism and magmatic related ore-forming fluids in northern Peru:

1. Palaeogene magmatic rocks were generated within an immature volcanic arc and derived from a residue characterised by anhydrous minerals (i.e. olivine and pyroxene). These magmas contained a magmatic water content of ~3 wt % H_2O, and underwent anhydrous and possibly hydrous mineral fractionation. A lack of mineralisation during this interval possibly relates to the dry nature of the mantle and melts.

2. Porphyry Cu deposits are associated with early-middle Miocene hornblende-biotite diorite stocks. These magmas were derived from large degrees of partial melting (~50%). The hydrous melts (> 3 wt % H_2O) equilibrated in the upper mantle with an amphibole-dominated residue. Replenishment of deep crustal ponds by primitive parental melts contributed significant amounts of magma and sulphur to the evolving

magma chamber. These hydrous sulphur-rich melts rose rapidly through the crust, which resulted in minimal crustal assimilation.

3. Late Miocene high-sulphidation deposits formed during cessation of uplift and crustal thickening in the Peruvian Andes that caused lowering of the crust-mantle boundary to present day depths (i.e. ~40 km). This resulted in a change of the residual mineralogy from amphibole to amphibole + garnet. The onset of a flat subduction zone also coincided with formation of the epithermal systems.